Title

iPSC-Derived Human Microglia-like Cells to Study Neurological Diseases

Journal

Neuron, 94(2)

ISSN

0896-6273

Authors

Abud, Edsel M

Ramirez, Ricardo N

Martinez, Eric S

et al.

Publication Date

2017-04-01

DOI

10.1016/j.neuron.2017.03.042

iPSC-derived human microglia-like cells to study neurological diseases.

Edsel M. Abud[1,2,3], Ricardo N. Ramirez[4], Eric S. Martinez[1,2,3], Luke M. Healy[5], Cecilia H.H. Nguyen[1,2,3], Sean A. Newman[2], Andriy V. Yeromin[6], Vanessa M. Scarfone[2], Samuel E. Marsh[2,3], Cristhian Fimbres[3], Chad A. Caraway [3], Gianna M. Fote[1,2,3], Abdullah Madany [11], Anshu Agrawal[7], Rakez Kayed[8], Karen H. Gylys[9], Michael D. Cahalan[6], Brian J. Cummings[2, 3, 10], Jack P. Antel[5], Ali Mortazavi[4], Monica J. Carson[11], Wayne W. Poon[3] *, and Mathew Blurton-Jones[1,2,3] *&

*Co-corresponding authors. &Lead Contact

[1]Department of Neurobiology & Behavior, [2]Sue and Bill Gross Stem Cell Research Center, [3]Institute for Memory Impairments and Neurological Disorders, [4]Department of Developmental and Cell Biology, [5]Neuroimmunology Unit, Department of Neurology and Neurosurgery, [6]Department of Physiology and Biophysics, [7]Department of Medicine, School of Medicine, [8]Department of Neurology, [9]UCLA School of Nursing, [10]Anatomy and Neurobiology, [11]Division of Biomedical Sciences.

[1,2,3,4,6,7, 10]University of California Irvine; Irvine, CA 92697, USA
[5]Montreal Neurological Institute and Hospital, McGill University, Montreal, Quebec, Canada
[8]George P. and Cynthia Woods Mitchell Center for Neurodegenerative Diseases, University of Texas Medical Branch, Galveston, TX, USA
[9]University of California, Los Angeles, Los Angeles, CA 90095, USA
[11]University of California, Riverside, Riverside, CA 92521, USA

*Shared correspondence:
Dr. Mathew Blurton-Jones and Dr. Wayne W. Poon
University of California, Irvine
3014 Gross Hall
845 Health Science Rd
Irvine, CA 92697-4545
Tel: 949-824-5243
Email: mblurton@uci.edu and wpoon@uci.edu

Summary

Microglia play critical roles in brain development, homeostasis, and neurological disorders. Here, we report that human microglial-like cells (iMGL) can be differentiated

from iPSCs to study their function in neurological diseases, like Alzheimer's disease (AD). We find that iMGLs develop *in vitro* similarly to microglia *in vivo* and whole transcriptome analysis demonstrates that they are highly similar to cultured adult and fetal human microglia. Functional assessment of iMGLs reveals that they secrete cytokines in response to inflammatory stimuli, migrate and undergo calcium transients, and robustly phagocytose CNS substrates. iMGLs were used to examine the effects of Aβ fibrils and brain-derived tau oligomers on AD-related gene expression and to interrogate mechanisms involved in synaptic pruning. Furthermore, iMGLs transplanted into transgenic mice and human brain organoids resemble microglia *in vivo*. Together, these findings demonstrate that iMGLs can be used to study microglial function, providing important new insight into human neurological disease.

Introduction

Microglia are the innate immune cells of the CNS and play important roles in synaptic plasticity, neurogenesis, homeostatic functions and immune activity. Microglia also play a critical role in neurological disorders, including AD, highlighting the need to improve our understanding of their function in both health and disease. Yet, studying human microglia is challenging because of the rarity and difficulty in acquiring primary cells from human fetal or adult CNS tissue. Therefore, there is a pressing need to develop a renewable source of human microglia, such as from induced pluripotent stem cells (iPSCs).

The challenges present in generating microglia from iPSCs are due to their unique developmental origin. Elegant lineage tracing studies show that microglia originate from yolk sac erythromyeloid progenitors (EMP) generated during primitive hematopoiesis (Ginhoux et al., 2010, Kierdorf et al., 2013, Schulz et al., 2012). EMPs further develop to early primitive macrophages that migrate into the developing neural tube, and become microglial progenitors (Kierdorf et al., 2013, Prinz and Priller, 2014). Microglia progenitors then mature and develop ramified processes used to survey their environment, facilitate CNS development, modulate synaptic plasticity, and respond to CNS injury and pathology. Recently, murine studies identified key cytokines, cell

receptors, and transcription factors required for microglia development and survival *in vivo*. These factors include IL-34 and TGFβ-1 (Wang et al., 2012, Greter et al., 2012, Yamasaki et al., 2014, Butovsky et al., 2014). Therefore, there exists a potential for guiding iPSC differentiation to human microglia *in vitro* by providing cues that mimic the environment present in the developing embryo.

The generation of patient-derived iPSCs has facilitated new opportunities to examine the relationships between genetic risk factors and disease. Recently, genome wide association studies (GWAS) have identified several genes expressed by microglia that are associated with the risk of developing late-onset AD (LOAD). The role of these genes in microglial function and AD are just beginning to be examined in mouse models, but the generation of human microglia-like cells would allow for the interrogation of human-specific genes that cannot be modeled in mice.

In AD, microglia cluster around beta-amyloid plaques highlighting their inability to clear beta-amyloid (Hickman et al., 2008, Liu et al., 2010). Microglia are also implicated in the neuroinflammatory component of AD etiology, including cytokine/chemokine secretion, which exacerbate disease pathology (Guillot-Sestier and Town, 2013). Furthermore, AD GWAS genes like TREM2 and CD33 are influenced by AD pathology and likely play a role in AD progression. Thus, there is a pressing need to further our understanding of human microglia and the influence of both pathology and disease-associated genes on microglial function. Addressing this critical need, we report the effective and robust generation of human iPSC microglial-like cells (iMGLs) that resemble fetal and adult microglia and demonstrate their utility in investigating neurological diseases like AD.

Results

Human microglia-like cells are generated from iPSCs.

A two-step fully-defined protocol was developed to efficiently generate microglia-like cells (iMGLs) from iPSCs in just over five weeks (**Figure 1A**). Importantly, we have used this approach to successfully produce iMGLs from 10 independent iPSC lines (**Figure S1A-C**). A critical prerequisite is the robust differentiation of iPSCs to hematopoietic

progenitors (iHPCs), which recapitulates microglia ontogeny as iHPCs represent early primitive hematopoietic cells derived from the yolk sac that give rise to microglia during development (Ginhoux et al., 2010, Kierdorf et al., 2013). Our protocol (depicted in **Figure 1Bi**) yields primitive iHPCs that are $CD43^+/CD235a^+/CD41^+$ (Sturgeon et al., 2014, Kennedy et al., 2007) after 10 days. FACS sorting for $CD43^+$ cells reveal that our approach produces iHPCs with a >90% purity (**Figure 1Bii)**. Interestingly, the resulting iHPCs resembled a commercial source (Cellular Dynamics International) and represent the hematopoietic progenitor used to generate iMGLs.

Next, $CD43^+$ iHPCs were grown in serum-free differentiation medium (formulated in house) containing CSF-1, IL-34, and TGFβ1. By day 14, cells expressed the myeloid-associated transcription factor PU.1 and the microglia-enriched protein TREM2 (**Figure 1A iii)** demonstrating an early commitment toward microglial fate. Because this protocol yields large amounts of iMGLs, we were able to follow their development *in vitro* characterizing them every 4 days by flow cytometry. Day 14 early iMGLs were $c\text{-}kit^-/CD45^+$ **(Figure 1C)**, suggesting commitment towards a myeloid lineage. Additionally, cells can be further subdivided into $CD45^+/CX3CR1^-$ (A1) and $CD45^+/CX3CR1^+$ (A2) populations; similar to developing microglial progenitors identified *in vivo (Kierdorf et al., 2013)*. CD45 expression was consistently monitored in developing iMGLs and compared to monocyte-derived macrophages (MD-Mφ). While CD45 expression increased with maturation, levels never reached that of macrophages (**Figure 1D**), consistent with murine development (Kierdorf et al., 2013). A small population of iMGLs (~10%) also expressed intermediate CD11b levels by day 14 that also increased as cells matured, but again never reached macrophage levels (**Figure 1E, F).**

By day 38, iMGLs resemble human microglia, but not monocytes nor macrophages by cytospin/Giemsa staining (**Figure 1G**) and express many other microglial-enriched proteins including MERTK, ITGB5, CX3CR1, TGFBR1, and PROS1 protein (**Figure 1I1H, Figure 4S**). Like murine microglia development *in vivo*, iMGLs developing *in vitro* express PU.1, TREM2, and $CD11b^{int}/CD45^{low}$ **(Figure 1A iii, D-F)**. As iMGLs mature *in vitro,* they also become more ramified (**Figure 1A iv, 1H),** similar to microglia *in vivo.* Furthermore, purinergic receptor P2ry12 and Trem2 co-expression was enriched in

iMGLs when compared to monocytes and quantification reveals our protocol yielded iMGLs of high purity (>97%, n=5)(**Figure 1I; Figure S2A, B**). Genomic integrity was also maintained over the course of differentiation. Assessing copy number variants across all chromosomes demonstrate that extra chromosomal fragments were not acquired by iMGLs when compared to their respective iPSCs (n=6, **Figure S1D, E).** A comparison of a representative differentiation across the entire probeset (n=383, nCounter Human Karyotype Panel) revealed a high correlation between the iPSC and iMGL genomes (r^2 > 0.92, **Figure S1F**). Importantly, this protocol yields 30-40 million iMGLs from one million iPSCs, suggesting that our approach can be readily scaled-up for high content screening.

iMGLs resemble human fetal and adult microglia

Next, the iMGL transcriptome was profiled in comparison to human primary fetal microglia (Fetal MG) and adult microglia (Adult MG). We also examined $CD14^+/CD16^-$ monocytes (CD14 M), $CD14^+/CD16^+$ inflammatory monocytes (CD16 M), myeloid dendritic cells (Blood DCs), iHPCs, and iPSCs, to compare iMGLs to stem cells and other myeloid molecular signatures. Correlational analysis and Principal Component Analysis (PCA) revealed striking similarity of iMGLs (blue) to Fetal MG (orange) and Adult MG (green)(**Figure 2A; Figure S3A**). Furthermore, the first principal component PC1 (21.3 % variance, **Figure 2A** arrows) defines the differentiation time-series from iPSC through iHPC to our iMGL cells while PC2 and PC3 define the dendritic and monocyte trajectories, respectively. Biclustering analysis using 300 microglial, macrophage, and other immune related genes adapted from previous studies (Butovsky et al., 2014, Hickman et al., 2013, Zhang et al., 2014) identified similarities between groups and highlighted common gene clusters, but also uncovered differences between all groups. This analysis again showed that iMGLs cluster with microglia but are distinct from other myeloid cells, iHPCs and iPSCs (**Figure 2B**).

Importantly, iMGLs, Fetal MG, and Adult MG express canonical microglial genes such as P2RY12, GPR34, C1Q, CABLES1, BHLHE41, TREM2, ITAM PROS1, APOE, SLCO2B1, SLC7A8, PPARD, and CRYBB1 (**Figure 2C; Table 1**)**.** When compared to

monocytes, iMGLs express the myeloid genes, RUNX1, PU.1, and CSF1R (**Figure S3C**), but do not express monocyte-specific transcription factors, IRF1, KLF4, NR4A1 (Lavin et al., 2014, Abdollahi et al., 1991, Hanna et al., 2011) (**Figure S3D**). Differential analysis between iMGLs, CD14 M, and CD16 M **(Figure SF3F)** further emphasizes that iMGLs predominantly express microglial genes (greater than two-fold change and $p<0.001$) including CX3CR1, TGFBR1, RGS10, and GAS6, but not monocyte and macrophage genes KLF2, TREM1, MPO, ITGAL, and ADGRE5. At the protein level, iMGLs, like primary microglia are $CD45^{lo}$ compared to $CD45^{hi}$ MD-Mφ, and express the microglia surface proteins Cx3cr1, TgfbRr1, P2ry12 and Pros1 (**Figure S2 and S4A).** Collectively, unbiased whole-transcriptome analysis strongly establishes iMGLs as a cell model that highly resembles primary human microglia that can be used to study microglia physiology and function in human health and disease.

Whole transcriptome differential analysis revealed increased expression of 1957 genes and 1071 genes in iMGLs when compared to Fetal MG or Adult MG, respectively. We also observed decreased expression of 1916 genes compared to fetal MG and 1263 genes compared to Adult MG. Enrichment analysis between iMGLs and primary microglia show that iMGLs are enriched for pathways involving cell cycle processes, migration, microtubule cytoskeletal organization, and inflammatory response, but do not differ in core myeloid GO terms (Tables 4-6). These terms reflect expected processes in which iMGLs are cued to respond to the environment and a capacity for renewal and maturation that have previously been reported in cultured microglia (Butovsky et al., 2014). Differential analysis between Fetal MG and Adult MG identified pathways related to responses to environment like migration and phagocytosis regulation, but not key myeloid genes in Fetal MG. Adult MG enrichment includes ECM organization, nervous system regulation, cell adhesion, and negative regulation of cell proliferation.

Functional validation of iMGLs.

We next validated iMGLs as surrogates of microglia using both functional and physiological assays. To this end, we measured cytokine/chemokine secretion by iMGLs stimulated by Lipopolysaccharide (LPS), and by IL-1β and IFNγ, two cytokines that are

elevated in AD patients and mouse models (Abbas et al., 2002, Blum-Degen et al., 1995, Patel et al., 2005, Wang et al., 2015). Basally, iMGLs secrete 10 of the examined cytokines at low but detectable levels (**Table 2**). However, in response to IFNγ or IL-1β, iMGLs secrete 8 different chemokines including TNFα, CCL2, CCL4, and CXCL10. As expected, iMGLs robustly responded to LPS with induction of all measured cytokines except for CCL3 (**Table 2** for values). Collectively, iMGLs differentially release cytokines/chemokines based on their cell-surface receptor stimuli, a finding that closely aligns with the responses observed in acutely isolated primary microglia (Rustenhoven et al., 2016).

Because iMGLs express the microglial-enriched purinergic receptor P2ry12, which can sense extracellular nucleotides from degenerating neurons and has been shown to be critical for microglial homeostatic function (De Simone et al., 2010, Moore et al., 2015) (**Figure 1H and 2C**), ADP-P2ry12 mediated chemotaxis and calcium transients were assessed. We found that iMGLs migrate robustly in response to ADP and ADP also triggered calcium transients (**Figure 3D, E**), which can both be negated by a P2ry12-specific inhibitor, PSB0739. These physiological findings further underscore that iMGLs express functional surface receptors, enabling quantitative analyses of microglial physiology.

Microglia along with astrocytes, also play a critical role in synaptic pruning (Aguzzi et al., 2013, Paolicelli et al., 2011, Stephan et al., 2012). Because *in vitro* synaptosome phagocytosis assays are an established surrogate to study pruning, we quantitatively assessed the ability of iMGLs to phagocytose human synaptosomes (hS). In comparison to MD-Mφ, iMGL phagocytosis of pHrodo-labeled hS was less robust (**Figure 3F, G**). However, iMGLs preferentially internalized hS when compared to *E. coli* particles and normalized to MD-Mφ (Supplementary **Figure 4D, E**) supporting the notion that iMGLs and microglia are more polarized toward homeostatic functions than MD-Mφ.

As iMGLs and primary microglia express both C1q and CR3 (CD11b/CD18 dimer), we used iMGLs to assess whether synaptic pruning in human microglia primarily involves

this pathway as seen in mice (Chung et al., 2013). Using an additive-free CD11b antibody, iMGL phagocytosis of hS was significantly reduced (-40.0%, ***p<0.0001) (**Figure 3H, I**)**.** In contrast, an inhibitor of MERTK (UNC569), also implicated in synaptic pruning, only marginally decreased iMGL hS phagocytosis (-12.6%, *p<0.05)(**Figure 3H, I**). Similar to studies in murine KO models, our data indicates that MERTK plays a minor role in human microglia-mediated synaptic pruning (Chung et al., 2013), whereas C1q/CR3 is integral for microglia-mediated synaptic pruning in humans.

Utility of iMGLs to study Alzheimer's disease

Impaired microglia clearance of beta-amyloid (Aβ) is implicated in the pathophysiology of AD and strategies to enhance clearance of AD pathology are being actively pursued by biopharma. Therefore, we examined whether iMGLs can phagocytose Aβ or tau, two hallmark AD pathologies. Similar to primary microglia, iMGLs internalize fluorescently labeled fibrillar Aβ (**Figure 4B**, bottom). iMGLs also recognize and internalize pHrodo-labled brain–derived tau oligomers (BDTOs) (**Figure 4B**, top). Fluorescence emitted indicates trafficking of pHrodo-conjugated BDTOs to the acidic lysosomal compartment showing that iMGLs can actively ingest extracellular tau that may be released during neuronal cell death (Villegas-Llerena et al., 2015) and support recent findings that microglia may play a role in tau propagation in AD and other tauopathies (Asai et al., 2015). Together, these findings suggest that iMGLs could be utilized to identify compounds in high-throughput drug-screening assays that enhance Aβ degradation or block exosome-mediated tau release.

Microglia genes are implicated in late onset AD, yet how they modify disease risk remains largely unknown. Thus, we utilized iMGLs to begin investigating how these genes might influence microglia function and AD risk. Hierarchical clustering using just these 25 AD-GWAS genes also demonstrates that iMGLs resemble microglia and not peripheral myeloid cells (**Figure 4A**). In their investigated basal state, iMGLs and microglia express many AD-GWAS-related genes including those without murine orthologs i.e. CD33, MS4A4A, CR1. Thus, iMGLs can be used to study how altered expression of these genes influence microglia phenotype in a way that cannot be

recapitulated in transgenic mice. Next, we investigated how fAβ or BDTO treatment influences AD-GWAS gene expression in microglia (Villegas-Llerena et al., 2015). Following fAβ exposure, iMGLs increased expression of 10 genes (**Table 3**) including ABCA7 (5.79 ± 0.44), CD33 (6.02 ± 0.41), TREM2 (4.86 ± 0.50, and APOE (2.52 ± 0.19), genes implicated in Aβ clearance/degradation. BDTOs increased expression of 4 genes including CD2AP (4.62 ± 0.45), previously implicated in tau-mediated toxicity (Shulman et al., 2014). In addition, 6 genes were differentially elevated in fAβ compared to BDTOs (**Table 3**). Interestingly, CD33, TYROBP, and PICALM, genes more enriched in other myeloid cells at baseline, were upregulated by fAβ and BDTOs suggesting that proteinopathies may alter microglia phenotype to resemble invading peripheral myeloid cells (Stalder et al., 2005, Prinz et al., 2011, Chan et al., 2007). In addition to AD GWAS genes, iMGLs express other CNS disease-related genes including APP, PSEN1/2, HTT, GRN, TARDBP, LRRK2, C9orf72, SOD1, VCP, and FUS and therefore, can likely be used to study other neurological diseases such as ALS, HD, FTD, and DLB in which microglia play a prominent modulatory role (**Figure S5**).

iMGL maturation and homeostasis is modulated by a CNS environment

Neurons, astrocytes, and endothelial cells in the brain interact with microglia to influence gene expression and function. Our differentiation protocol attempted to recapitulate CNS cues present in the brain by including signals derived from these other cell types including CX3CL1, CD200, and TGFβ. Whole transcriptome RNA-seq analysis confirmed the importance of these factors for establishing microglia *in vitro* (**Figure S5**). TGFβ, a glia-derived cytokine, is needed for murine microglia development *in vivo* and in maintaining the microglial-specific transcriptome signature (Schilling et al., 2001, Butovsky et al., 2014, Abutbul et al., 2012). Differential gene expression analysis confirmed TGFβ's role in maintaining the human microglia transcriptome signature; 1262 genes were differentially expressed in iMGLs with TGFβ, whereas 1517 genes were differentially expressed in iMGLs after TGFβ removal (24 hours). Many of the differentially expressed genes are identified as core microglial signature targets including P2RY12, TGFβR1, and CD33, and transcription factors EGR1 and ETV5, and APOE (**Figure S5A-C).** Examination of gene ontology highlight neurodegenerative

disease pathways including AD, Parkinson's, and Huntington's diseases that are TGFβ dependent (**Figure S5D**). Furthermore, removal of TGFβ led to significant changes in many of the human microglia homeostatic targets also identified as AD GWAS loci genes including TREM2, APOE, ABCA7, SPI1 (CELF1 locus), PILRA (ZCWPW1 locus), and the HLA-DR and MS4A gene clusters ((Karch et al., 2016), suggesting many identified AD GWAS genes function in the maintenance of microglia homeostasis (**Figure S5E**) and underscoring the utility of iMGLs to interrogate AD GWAS gene function.

CX3CL1 and CD200 are both neuronal- and endothelial-derived cues that can further mature iMGLs toward an endogenous microglia phenotype. Differential whole transcriptome gene analysis reveal that the core microglia transcriptome signature was refractory to CX3CL1/CD200, but expression of select microglia-enriched genes, including catechol-*O*-methyltransferase COMT(Bennett et al., 2016), CD52, a cell surface receptor that binds Siglec-10 and interacts with DAP12 as part of the microglia sensome (Hickman et al., 2013), and HLA-DRB5, a member of the MHC II complex implicated in AD (**Figure S5C**), were still enhanced. While extensive differential gene expression was not observed, iMGLs not exposed to CD200 and CX3CL1 responded to fibrillary Aβ by suppressing many of the genes implicated in AD-risk (**Figure 4C, S6B**). Thus, exposure to soluble CNS factors, like CD200/CX3CL1, may allow for access to microglial-specific transcriptional regulator elements (enhancers and promoters), yet future studies are required to fully translate these observations.

Next, we examined whether iMGL maturation can be achieved with direct contact with the CNS environment. Therefore, iMGLs were cultured with rat-hippocampal neurons (21 DIV) to assess how iMGLs respond to neuronal surface cues (**Figure 5A**). Rat-hippocampal neurons were used because they readily form synapses in culture and can be generated with limited variability. iMGLs were subsequently separated from neurons by FACs with human specific CD45 and CD11b antibodies and profiled at the transcriptome level (**Figure 5B)**. Differential gene expression analysis revealed that neuronal co-culturing upregulated 156 and downregulated 244 iMGL genes (**Figure 5C and D**). FFAR2 and COL26A1 are two genes differentially expressed in iMGLs cultured

with only defined factors and indicate a developmentally primed microglia profile. In contrast, co-culturing microglia with neurons increased expression of Siglec11 and 12, human-specific sialic-acid binding proteins that interact with the neuronal glycocalyx, function in neuroprotection, and suppress pro-inflammatory signaling, and thus maintain a microglia homeostatic state (Wang and Neumann 2010) (Linnartz-Gerlach et al., 2014). Additionally, we saw increased expression of microglial genes CABLES1, TRIM14, MITF, MMP2, and SLC2A5. Overall, these results implicate both soluble and surface CNS cues as factors in microglia maturation (Biber et al., 2007) (**Figure 5E**, GO Terms, **Figure S6**).

A fundamental characteristic of microglia is the surveillance of the neuronal environment with their highly ramified processes. To investigate how iMGLs might interact within a human neuronal environment, iMGLs were cultured with hiPSC 3D brain-organoids (BORGs). BORGs include neurons, astrocytes, and oligodendricytes that self-organize into a cortical-like network, but lack microglia (**Figure 6B**). To test if iMGLs invade BORGs similarly to how microglia enter the developing neural tube (Rezaie and Male, 1999, Chan et al., 2007), iMGLs were added to BORG cultures. By day three, iMGLs had embedded into the BORGS and were no longer detectable within the media suggesting rapid iMGL chemotaxis toward neuronal cues (**Figure 6A i, ii, iii**). By day 7, the iMGLs (green) also tiled and extended varying degrees of ramified processes within the 3D organoid environment (**Figure 6B)**. iMGL projections were observed in a vast majority of cells and exhibited similar morphology to microglia *in vivo* (**Figure 6B).** To determine whether iMGLs respond to neuronal injury, BORGS were pierced with a 25-gauge needle (white long arrow, **Figure 6Ci).** After injury, iMGLs clustered near the injury site and at BORG edges (**Figure 6C ii)** and adopted a more amoeboid morphology, resembling “activated” microglia found in injured or diseased brains (Kettenmann et al., 2011) (**Figure 6Ciii)**. Collectively, these data demonstrate that iMGLs can integrate within an *in vitro* 3D neuronal environment, mature, ramify, and respond to injury similar to brain microglia.

Next, we sought to examine iMGLs within the context of a neuronal environment *in vivo*. To this end, iMGLs (day 38) were transplanted into the cortex of MITRG mice that are

Rag2-deficient and IL2r□-deficient mice and also express the human forms of four cytokines knocked-in (M-CSF^{h};IL-3/GM-CSF^{h};TPO^{h}), allowing for xenotransplantation and survival of myeloid and other leukocytes (Rongvaux et al., 2014)(**Figure 7**). Two months after transplantation, the extent of engraftment in MITRG cortices was assessed by immunohistochemistry. Human iMGLs were distinguished from endogenous microglia by using either human specific nuclear or cytoplasmic markers ku80 (hNuclei) and SC121 (hCyto), respectively. P2ry12 and human-specific Tmem119 antibodies were used to assess the homeostatic state and identity of transplanted microglia (Butovsky et al., 2014, Bennett et al., 2016, Haynes et al., 2006). Transplanted human iMGLs co-expressing both ku80 and P2ry12 were abundant within MITRG brains suggestive of their long-term engraftment potential (**Figure 7A-D**). Higher magnification images show P2ry12 expression in highly ramified iMGLs resembling quiescent cortical microglia in which the membrane distribution accentuates the finer extended processes (**Figure 7B-D**) (Baron et al., 2014). TMEM119 was also expressed in both hCyto^{+} soma and the processes of highly arborized iMGLs (**Figure 7E-H**). High magnification images of hCyto^{+} cells show Tmem119 is predominately membrane-bound and in agreement with published work (Bennett et al., 2016). Taken together, these findings suggest that long-term survival and engraftment of iMGLs result in highly branched microglia-like cells that express Iba1, P2ry12 and Tmem119, and resemble endogenous quiescent microglia. Also, the morphology and high expression of the homeostatic P2ry12 receptor suggests that transplanted iMGLs are actively surveying their neuronal environment that translates to their potential use in studying human microglia in mouse CNS-disease models.

To test this hypothesis, iMGLs were transplanted into the hippocampi of xenotransplantation-compatible AD mice, previously generated and characterized in our lab (Marsh et al., 2016), to examine how iMGLs interact with AD neuropathology *in vivo* (**Figure 7M-P**). Transplanted iMGLs engraft and migrate along white matter tracts, similar to microglia in development (**Figure 7M**). In many instances, iMGLs migrated and extended processes towards Aβ plaques to begin walling them off (**Figure 7N-P, and Supplementary Video 1**). A number of iMGLs also began to phagocytose fibrillar Aβ (**Figure 7N-P,S7E-H**). Similarly, human fetal microglia migrated towards Aβ,

extended processes, and phagocytosed Aβ when transplanted in the same AD transgenic model (**Figure S7A-D**).

Discussion

Here, we show that human microglia-like cells can be generated from iPSCs following a fully-defined and highly efficient protocol, which enables high purity (>97%) and robust scalability. Importantly, iMGLs are highly similar to cultured human adult and fetal microglia by both transcriptomic and functional analyses. Our whole-transcriptome PCA also highlights the differentiation trajectory of iPSCs toward iHPCs, and then iMGLs. Moreover, our series of microglial functional assays, only possible with a high yield and pure protocol, further strengthens how iMGLs can be used to investigate microglia genes implicated in disease and understand physiological function both *in vitro* and *in vivo.*

We also demonstrate the use of iMGLs to investigate human microglial function as a therapeutic target in human disease. A recent study implicated complement and increased microglia-mediated pruning of synapses early in AD (Hong et al., 2016a, Hong et al., 2016b). Here, we found that blocking CR3, via anti-CD11b, in iMGLs reduces phagocytosis of human synaptosomes. Our findings provide one of the first examples, to our knowledge, of quantitative evidence showing human microglia engulfing human synaptosomes predominately via the CR3 axis, as implicated by transgenic mouse studies (Hong et al., 2016a). Moreover, we highlight the utility of iMGLs to examine microglia-targeted AD therapies, such as anti-CD11b, in phagocytic assays and to potentially examine or validate other complement-targeted therapies in development.

Microglia mediate neuroinflammation through surveillance of their environment and by cell surface receptor activation. We therefore tested iMGL response to extracellular stimuli observed in AD, such as nucleotides leaked from degenerating neurons. Microglia sense ADP release via purinergic receptors and we likewise find that iMGLs robustly express functional P2ry12 and migrate and exhibit calcium influx via an ADP-P2ry12 receptor mechanism. Also, iMGLs secrete a variety of cytokines in response to

IFNγ, IL-1β, and LPS stimulation. Many of these cytokines are known to be highly elevated in neurological diseases and/or involved in the recruitment of peripheral immune cells into the CNS under pathological conditions (Stalder et al., 2005, Prinz et al., 2011, Rezaie and Male, 1999, Chan et al., 2007). Microglial-mediated cytokine secretion can further influence the inflammatory milieu in the CNS and thus represents an excellent therapeutic target for restoring CNS homeostatic balance. Together, migration, calcium imaging, and cytokine secretion assays not only validate iMGLs to be highly similar to brain-derived microglia but provide important functional assays to assess the role of microglia in neuroinflammation. Our data highlights the potential utility of iMGLs to identify therapeutic compounds via high throughput assessment of microglia physiology

Since the discovery of SNPs in immune genes as AD-risk factors, microglia have been further highlighted in human neurological health and disease. Several of these AD-GWAS genes, including CD33 and CR1, lack functionally-similar murine orthologs. Thus, iMGLs can be utilized to investigate how AD-GWAS genes change in human microglia when exposed to pathological AD proteins. To this end, iMGLs were used to examine for the first time, to our knowledge, how AD-GWAS genes change in response to either Aβ or tau.

We also highlight how neuronal co-culture can further modulate microglial gene expression and how interactions with the neuronal glycocalyx increase Siglec expression. Interestingly, iMGLs not cultured with neurons differentially expressed early microglia genes including FFAR2 (Erny et al., 2015, Matcovitch-Natan et al., 2016) suggesting that other factors are needed to further educate microglia as tissue-resident macrophages of the brain. In accordance with this notion, iMGLs cultured in 3D neuronal cultures, iMGLs actively migrate, tile and encompass the volume of the BORGs, extending processes reminiscent of early microglia development. We also show that iMGLs transplanted in mice, engraft, survive, and display characteristic ramified processes that have increased branch order complexity, closely resembling quiescent microglia (Andreasson et al., 2016). We also note that transplanted, highly ramified iMGLs were morphological heterogeneous within the brain (**Figure 7I-L**). This

morphological diversity is indicative of microglia responding to distinct cortical layers/brain-regions and potentially reflecting microglia subtypes found within the brain (Grabert et al., 2016). Our results also demonstrate that iMGLs can appropriately respond appropriately to the neurotoxic build-up of Aβ.

Overall, these results highlight the potential of a renewable source of patient-derived iMGLs for studying human microglial genes and functions in neurodegenerative diseases. Transplantation of iMGLs into various CNS disease mouse models will allow for the study of human microglial function in neurodegenerative disease *in vivo* that may be influenced by genetics and the inheritance of specific mutations. This platform will allow for the identification of potential novel microglial-based translational therapies, as recently discussed (Biber et al., 2016). Finally, while technical challenges exist for isolating microglia from both human brain and BORGS for study, the development of future tools will likely make it feasible to compare isolated microglia from BORGs with freshly isolated microglia to determine whether 3D organoid systems fully recapitulate the *in vivo* microglia signature. In summary, we demonstrate a methodology to generate human microglial-like cells in large quantities from renewable iPSCs that can be used as primary microglia surrogates.

Our study is one of the first to describe a protocol for generating microglial cells from induced pluripotent stem cells with the exception of a recently published resource from Muffat and colleagues, 2016 (Muffat et al., 2016). However, their approach uses hematopoietic cells derived from embryoid bodies (EB) as microglia precursors. One challenge with the use of an EB-based method and selection by cell adhesion (Muffat et al protocol) is the potential contamination by other cell types that spontaneously arise from EBs i.e. neuroectoderm including astrocytes. Thus, some questions remain in terms of yield, scalability, and purity using an EB-based method and whether the resulting cells can be used to interrogate microglial function in quantitative assays that require large numbers of pure microglia-like cells.

To this end, we highlight the high yield of iHPCs and iMGLs from iPSCs with this protocol and the availability of a commercial HPC source that can be readily

differentiated to iMGLs. We also show that iMGLs phagocytose a variety of neuronal substrates including beta-amyloid, brain-derived tau oligomers, and human synaptosomes, and demonstrate that synaptic pruning by human microglia is mediated via CR3, highlighting their use in discovering and validation of microglia-targeted therapies. Furthermore, previous and newly identified AD-GWAS genes including novel TREM2 variants associated with AD-risk (Sirkis et al., 2016) can be studied with iMGLs. Because many AD-GWAS genes suggest microglia-neuronal crosstalk (e.g. TREM2-Lipids and APOE/J, CD33-Sialic Acid), we also show that iMGLs can be studied with neurons and glia by examining how both rodent and human neuronal cells influence microglia phenotype and function. As expected, iMGLs gene profiles shift toward a neuronal-centric phenotype and respond appropriately to injury in 3D cell culture and beta-amyloid plaques in AD transgenic mice brains. Together, our fully-defined protocol yields highly-pure microglia-like cells that provide a platform to investigate human microglia function for a broad range of CNS development, homeostatic function, and neurological diseases applications. While the validation of iMGLs as microglia surrogates raised several new and exciting questions related to microglia biology in development, health and disease, this new renewable resource will allow for those questions to be further addressed by the field.

Author Contributions:

E.M.A. and M.B-J. conceived the project. E.M.A., R.N.R., E.S.M., M.J.C., W.W.P., and M.B-J. designed and supervised experiments, and interpreted results. E.M.A and E.S.M. designed the differentiation method and growth of iHPCs. E.M.A designed the differentiation method and growth of iMGLs. A.A. provided DC RNA. L.M.H. and J.P.A. provided fetal and adult microglia RNA. R.N.R., E.M.A., and W.W.P. designed and performed transcriptome analysis with input from A.M. E.M.A., E.S.M., and W.W.P. designed, performed, and analyzed functional assays. S.A.N. and B.J.C. developed the 3D Borgs. E.M.A. and A.V.Y. designed, performed and analyzed calcium imaging with input from M.D.C. E.M.A. and V.S.M. designed, performed, and analyzed flow cytometer

studies. E.M.A., M.B.J., and S.E.M. performed immunofluorescence imaging and IMARIS analysis. A.Ma generated preliminary data. K.G.H. isolated and C.F. prepared, processed, and labeled synaptosomes. C.A.C. prepared neuronal cultures. R.K. isolated and characterized BDTOs and C.F. processed and labeled BDTOs. E.M.A. and W.W.P. performed all other experiments and analysis. C.H.H.N. and G.M.F. assisted with cell culture, sample prep, and data analysis. E.M.A., R.N.R., E.S.M., W.W.P., and M.B-J. wrote the paper and all authors provided feedback.

Acknowledgements: This work was supported by NIH AG048099 (MBJ) and AG016573 (MBJ and WWP), CIRM RT3-07893 (MBJ), Alzheimer's Association BFG-14-317000 (MBJ), UCI MSTP (EMA and GMF), a Stem Cell Research Center SEED grant for Borgs (B.J.C.) and a Burden Fellowship (A.M.). We thank UCI Genomics Core, the Institute for Immunology, and Dr. Jennifer Atwood.

Accession Numbers

We deposited the RNA-sequence data in the NCBI GEO database: GSE89189

Conflict of Interests

The authors declare no conflict of interests.

Figures and Legends

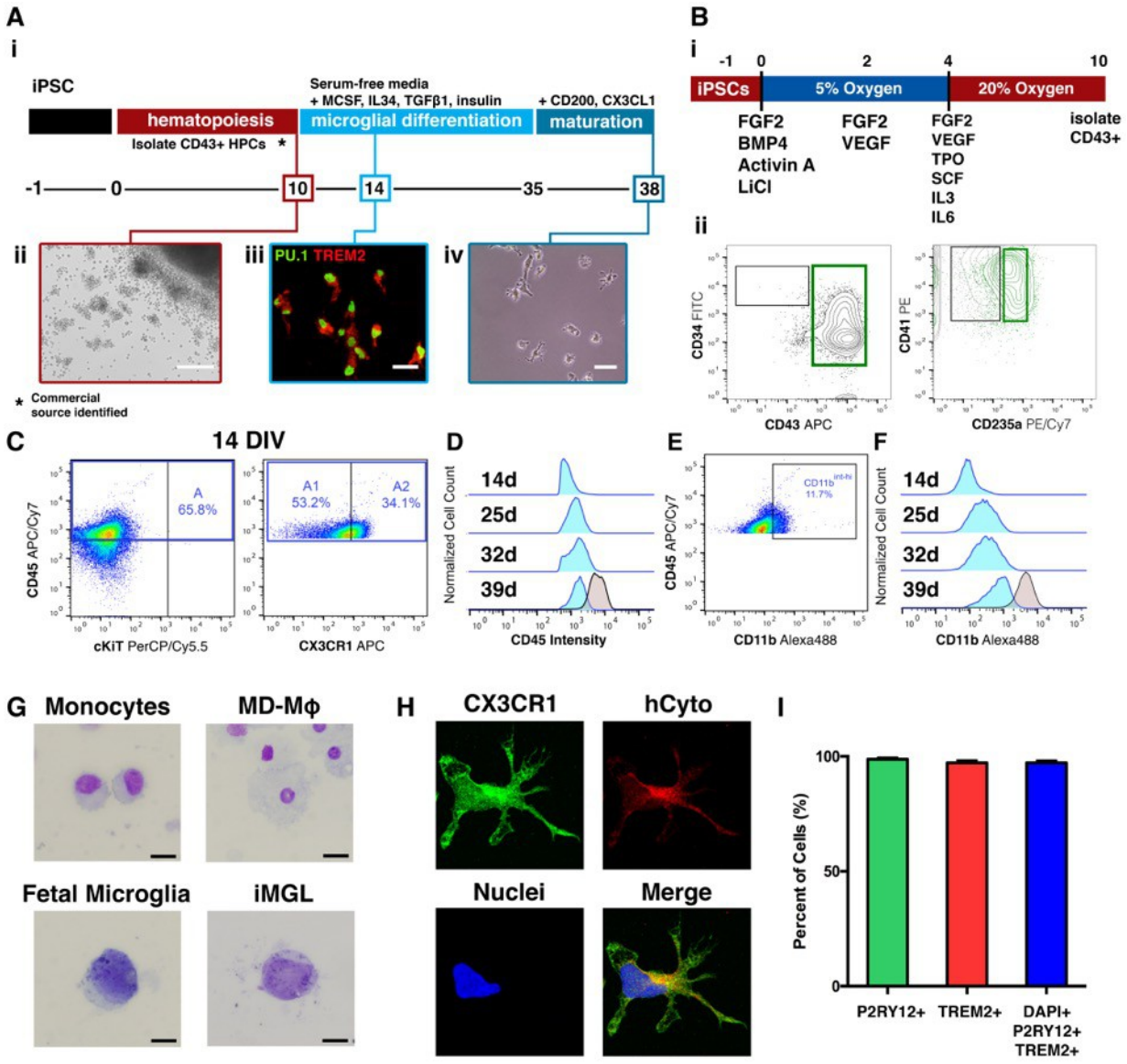

Figure 1. Differentiation of human iPSC derived microglia like cells (iMGLs). (A) Schematic of fully-defined iMGL differentiation protocol. (**i**) Human iPSCs are differentiated to CD43^{+} iHPCs for 10 days and then cultured in serum-free microglia differentiation media containing human recombinant MCSF, IL-34, and TGFβ-1. Differentiation is carried out for an additional 25 days after which iMGLs are exposed to human recombinant CD200 and CX3CL1 for 3 days. (**ii**) Representative image of iHPCs in cell culture at day 10. Scale bar = 100 µm. (**iii**) By day 14, iMGLs express PU.1 (green) and TREM2 (red). Scale bar = 50 µm. (**iv**) Representative phase contrast image of iMGL at day 38. (**B**) Schematic of differentiation of iPSCs to iHPCs. (**i**) Single-cell

iPSCs are differentiated in a chemically defined media supplemented with hematopoietic differentiation factors and using 5% O_2 (4 days) and 20% O_2 (6 days). (**ii**) After 10 days, $CD43^+$ iHPCs are $CD235a^+/CD41a^+$(**C**) iMGLs develop from $CD45^+/CX3CR1^-$ (A1) and $CD45^+/CX3CR1^+$ (A2) progenitors. (**D**) CD45 fluorescence intensity shows that iMGLs (blue) maintain their $CD45^{lo\text{-}int}$ profile when compared to monocyte-derived macrophage (MD-Mφ). (**E**) iMGL progenitors are $CD11b^{lo}$ and increase their CD11b expression as they mature. At 14 DIV, a small population (~11%) cells with $CD11b^{int\text{-}hi}$ are detected. (**F**) CD11b fluorescence intensity demonstrates that CD11b expression increases as iMGLs age, resembling murine microglial progenitors identified by Kierdorf, et al 2013. (**G**) Mary-Grunwald Giemsa stain of monocytes, MD-Mφ, fetal microglia, and iMGLs using. Both fetal microglia and iMGL exhibit a high nucleus to cytoplasm morphology compared to monocytes and MD-Mφ. Scale bars = 16 µm. (**H**) iMGLs also exhibit extended processes and express CX3CR1 (green) and a human cytoplasmic marker (hCyto, SC121; red). **(I**) Differentiation yields >97.2% purity as assessed by co-localization of microglial-enriched protein P2RY12 (green), microglial-enriched TREM2 (red) and nuclei (blue) (n=5 representative lines). *See also Figure S1 and S2.*

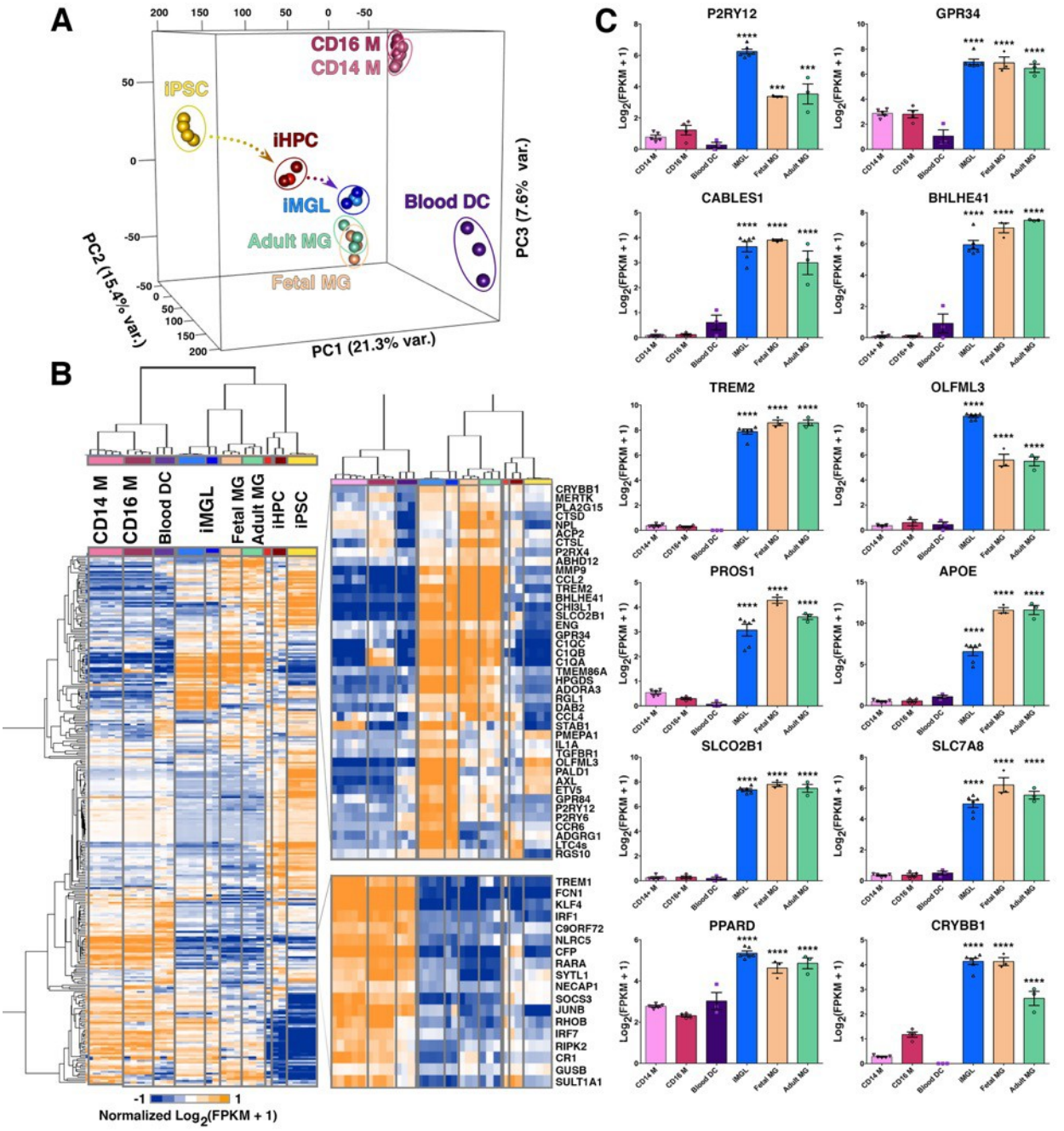

Figure 2. iMGL transcriptome profile is highly similar to human adult and fetal microglia. (**A**) 3D Principal Component Analysis (PCA) of iMGLs (blue), human adult microglia (Adult MG; green), human fetal microglia (Fetal MG; beige), $CD14^{+}/CD16^{-}$ monocytes (CD14 M; pink), $CD14^{+}/16^{+}$ monocytes (CD16 M; maroon), blood dendritic cells (Blood DC; purple), iHPCs (red), and iPSCs (yellow) (FPKM ≥ 1, n=23,580 genes). PCA analysis reveals that iMGL cluster with Adult and Fetal MG and not with other myeloid cells. PC1 (21.3% var) reflects the time-series of iPSC differentiation to iHPC

(yellow arrow) and then to iMGLs (blue arrow). PC2 (15.4% var) reflects trajectory to Blood DCs. PC3 (7.6% var) reflects trajectory to monocytes (**B**) Heatmap and biclustering (Euclidean-distance) on 300 microglia, myeloid, and other immune related genes (Butovsky et al., 2014, Hickman et al., 2013, Zhang et al., 2014). A pseudo-count was used for FPKM values (FPKM +1), log_2-transformed and each gene was normalized in their respective row (n=300). Representative profiles are shown for genes up and down regulated in both human microglia (fetal/adult) and iMGLs. (**C**) Bar graphs of microglial-specific or –enriched genes measured in iMGL, Fetal and Adult MG, Blood DC, CD14 M, and CD16 M as [Log_2 (FPKM +1)] presented as mean ± SEM. Data that was analyzed using one-way ANOVA followed by Tukey's corrected multiple comparison *post hoc* test. Statistical annotation represents greatest p-value for iMGL, Fetal MG, and Adult MG to other myeloid cells. CD14 M (n=5, CD16 M (n=4), Blood DC (n=3), iMGL (n=6), Fetal MG (n=3), and Adult MG (n=3). *p<0.05, **p<0.01, ***p<0.001, ****p<0.0001. Complete statistical comparisons are provided in **Table S1**. *See also Figure S2 and S3.*

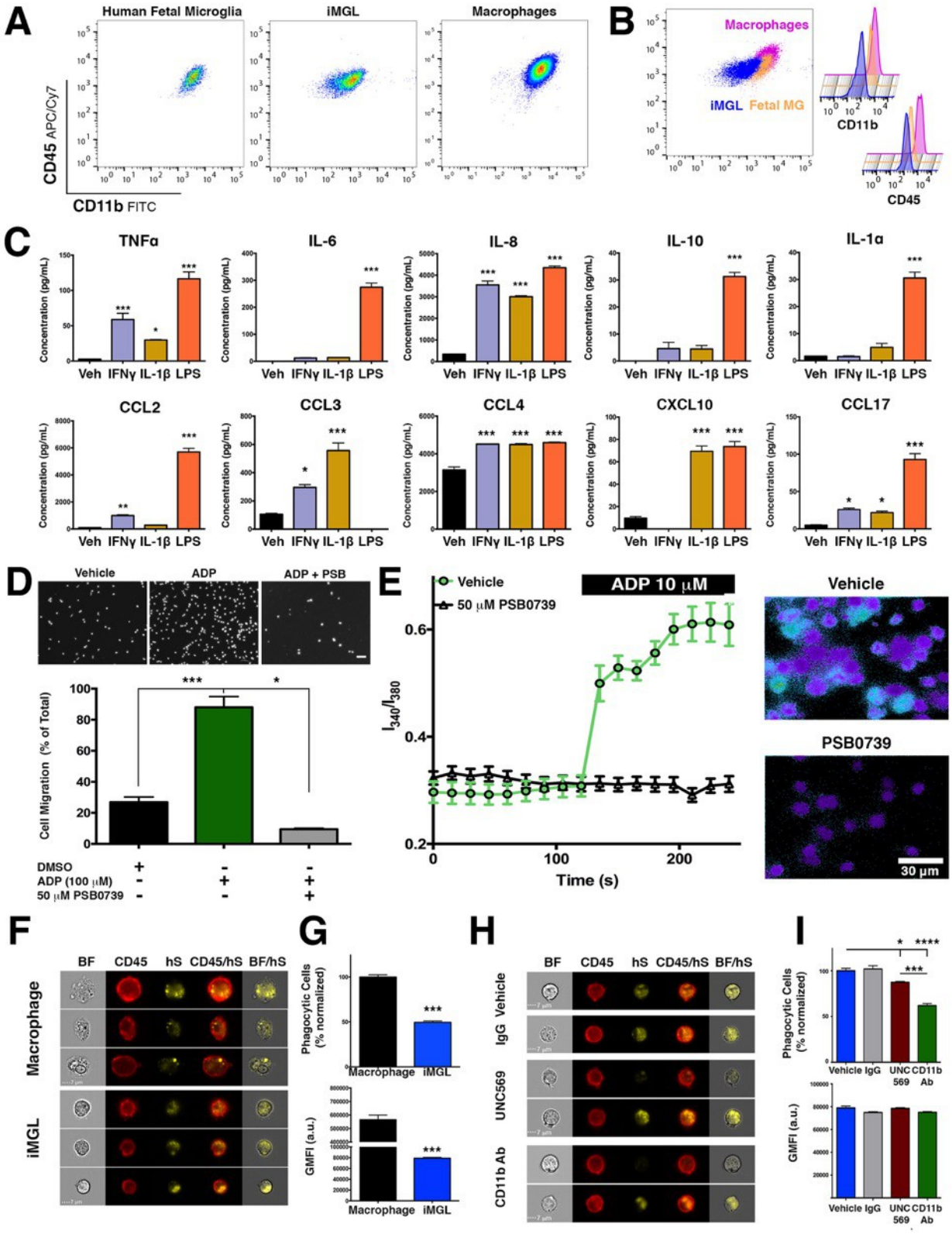

Figure 3. iMGLs are physiologically functional and can secrete cytokines, respond to ADP, and phagocytose human synpatosomes. (A-B) By flow cytometry

analysis, iMGL (blue) are $CD45^{lo\text{-}int}$ similar to fetal MG (orange) but different from $CD45^{hi}$ MD-Mφ (fuchsia). (**B**) Histogram of CD11b intensity (left) reveals that fetal MG express slightly more CD11b than iMGL but less than MD-Mφ. (**C**) iMGLs secrete cytokines and chemokines when stimulated for 24 hours with either IFNγ (20 ng/ml), IL-1β (20 ng/ml), or LPS (100 ng/ml) by ELISA multiplex. (**D**) ADP (100 μM) induces iMGL migration in a trans-well chamber (5 μm). Pre-exposure to the P2ry12 antagonist, PSB0739 (50 μM, 1 hr) completely abrogates ADP-induced iMGL migration (***p<0.0001). (**E**) ADP induces calcium flux in iMGLs via P2ry12 receptors. (*Left*) Exposure to ADP leads to elevated calcium influx (I_{340}/I_{380} ratio) in vehicle group (green trace) but not in PSB0739-treated group (black trace). (*Right*) Representative images of ADP-induced calcium flux at 240 s in vehicle (top) and PSB0739 (bottom). (**F**) iMGLs phagocytose human brain-derived synaptosomes (hS). Representative images captured on Amnis Imagestream display phagocytosis of hS by MD-Mφ and iMGLs. (**G**) Quantification of phagocytosis shows that iMGLs internalize hS at 50% of macrophage capacity (p<0.0001). **(H**) Representative images of iMGL phagocytosis of hS in the presence of either a MerTK inhibitor UNC569 (top) or anti-CD11b antibody (bottom). (**I**; top) iMGL phagocytosis of hS phagocytosis is reduced byby approximately 12% (burgundy bar, p<0.05) by blocking MerTK, but 40% (p<0.0001, green bar) by inhibiting CR3 via CD11b blockade. (**I**; bottom) Sub-analysis of iMGLs exhibiting a phagocytic event reveals similar average amounts of internalization across treatment groups (p=0.1165). All histograms reported as mean ± SEM. Cytokine and migration assays one-way ANOVA, followed by Dunnett's multiple-comparison *post-hoc* test, ***p<0.0001, **p<0.001, *p<0.05; Cytokine assay: n=3 wells/group. Migration Assay: n=5 fields /condition. Calcium assay: vehicle (n=37 cells), PSB0739-treated (n=17 cells), I_{340}/I_{380} represented as mean ± SEM at each time point. Phagocytosis assay: MD-Mφ vs iMGL: Unpaired t-test, **p<0.001, n=3 wells/group. MERTK and CR3 assay, one-way ANOVA, followed by Tukey's multiple-comparison *post-hoc* test, ***p<0.0001; n= 6 for vehicle, n=3 wells/group. *See also Figure S4.*

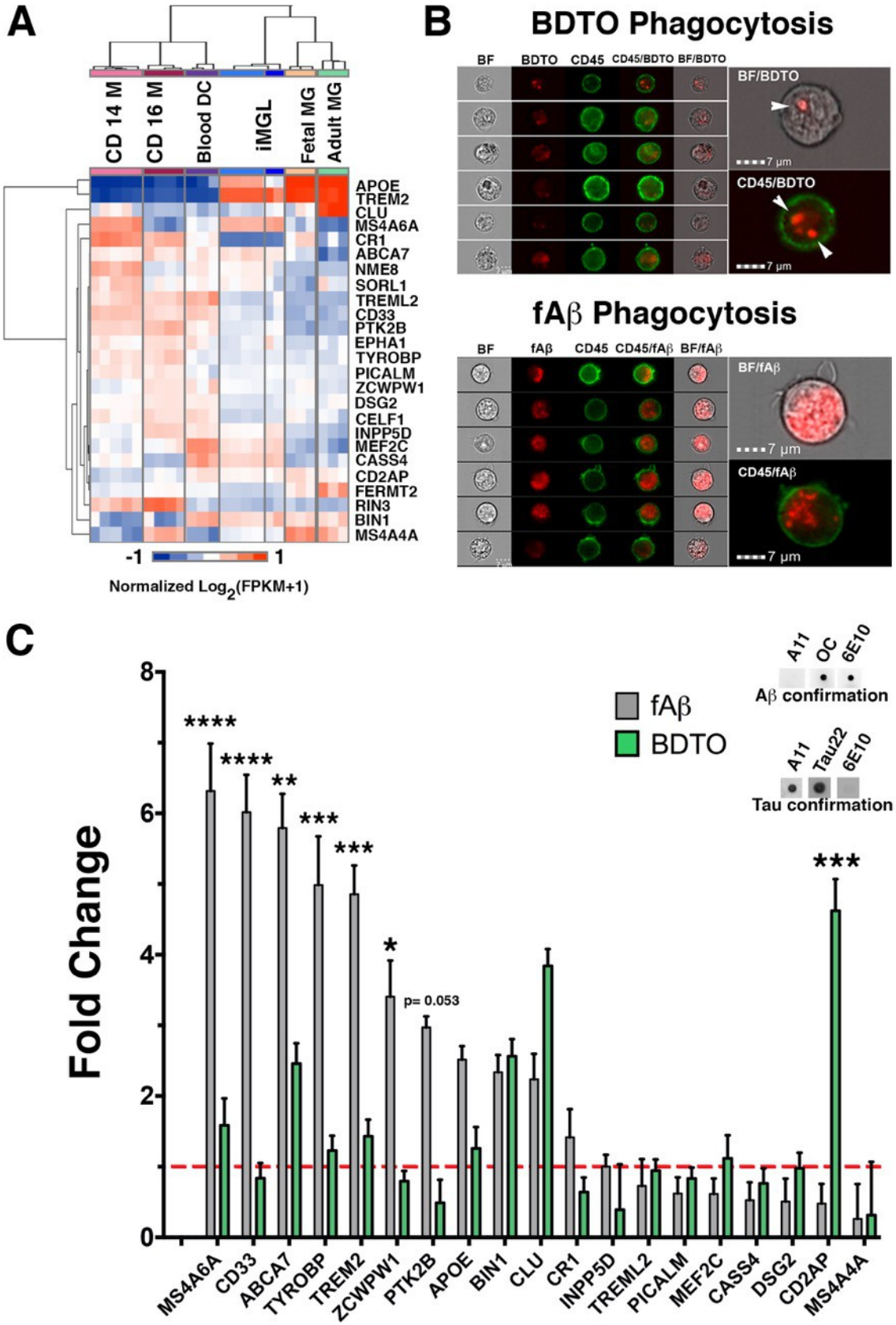
A
CD 14 M
CD 16 M
Blood DC
iMGL
Fetal MG
Adult MG
APOE
TREM2
CLU
MS4A6A
CR1
ABCA7
NME8
SORL1
TREML2
CD33
PTK2B
EPHA1
TYROBP
PICALM
ZCWPW1
DSG2
CELF1
INPP5D
MEF2C
CASS4
CD2AP
FERMT2
RIN3
BIN1
MS4A4A
-1
1
Normalized Log2(FPKM+1)
B
BDTO Phagocytosis
BF
BDTO
CD45
CD45/BDTO
BF/BDTO
7 µm
fAβ Phagocytosis
fAβ
CD45/fAβ
BF/fAβ
C
Fold Change
fAβ
BDTO
A11
OC
6E10
Aβ confirmation
Tau22
Tau confirmation
p= 0.053
MS4A6A
CD33
ABCA7
TYROBP
TREM2
ZCWPW1
PTK2B
APOE
BIN1
CLU
CR1
INPP5D
TREML2
PICALM
MEF2C
CASS4
DSG2
CD2AP
MS4A4A

Figure

4. Alzheimer Disease risk factor GWAS genes can be investigated using iMGLs and high throughput genomic and functional assays. (**A**). Heatmap of 25 immune genes with variants associated with *LOAD* reveals that major risk factors APOE and TREM2 are highly expressed in iMGLs, Adult MG, and Fetal MG. (**B**) iMGLs internalize fluorescent-labeled fAβ and pHrodo-dye BDTO. Representative images captured on Amnis Image StreamX Mark II. (**C**) iMGLs were exposed to unlabeled fAβ (5 μg-ml^{-1}) and BDTOs (5 μg/ml) for 24 h and mRNA expression of 19 GWAS genes was assessed via qPCR array. fAβ treatment elevated the expression of 10 genes above 2-fold compared to vehicle, including MS4A6A (6.3 fold), CD33 (6.1 fold), ABCA7 (5.8 fold), TYROBP (4.98) and TREM2 (4.85 fold). Whereas, BDTO exposure elevated the expression of 4 genes above 2-fold compared to vehicle. 6 genes were differentially expressed in fAβ compared to BDTO. fAβ and BDTO preparations were confirmed via dot-blot analysis with conformation structural specific antibodies for oligomers (A11), fibrils (OC) and non-structural-specific antibodies for human Aβ (6E10) and tau oligomers (Tau22). Target genes were normalized to GAPDH and compared to vehicle expression by ΔΔCt. Bars show expression fold mean ± SEM. Red hash bar is ΔΔCt = 1Two. Two-Way ANOVA, followed by Sidak's multiple-comparison *post-hoc* test, ***p<0.0001, **p<0.001, *p<0.05; n=6 wells/group. Data represented as mean ± SEM. *See also Figure S5 and S6*.

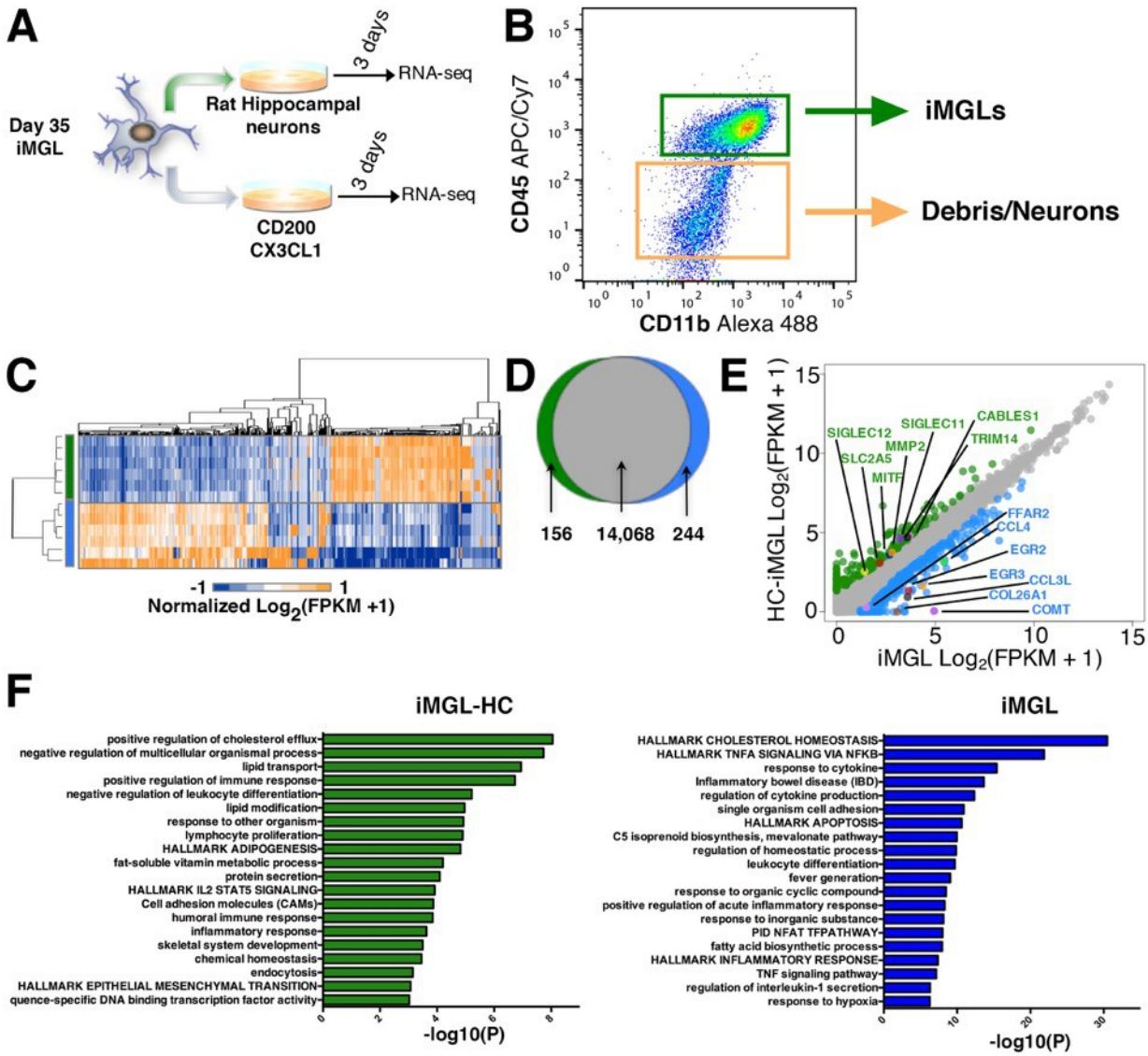

Figure 5. iMGLs gene profiles are responsive to neuronal environment. (**A**) Schematic of iMGL co-culture with or without rat hippocampal neurons. (**B**) iMGLs co-cultured with neurons were collected, assessed by flow cytometry and transcriptomes evaluated via RNA-sequencing. (**C**) Heat map of iMGLs and iMGL-HC gene expression highlights uniquely enriched genes. (**D**) Differential gene expression analysis highlights 156 upregulated and 244 downregulated genes in iMGL-HCs. (**E**) Scatter plot of differentially expressed genes [> 2 Log_2(FPKM+1)] highlight TRIM14, CABLES1, MMP2, SIGLEC 11 and 12, MITF, and SLC2A5 being enriched in iMGL-HCs, suggesting that iMGLs respond appropriately to a neuronal environment. Cells cultured alone are enriched for COMT, EGR2, EGR3, and FFAR2 suggesting a primed microglia

phenotype. (**F**) GO and pathway terms from differential gene expression analysis of iMGLs cultured with hippocampal neurons. Genes upregulated in iMGL-HC are associated with 20 statistically significant pathway modules (green histogram) including positive cholesterol efflux, lipid transport, positive regulation of immune response, negative regulation of leukocyte differentiation and cell adhesion molecules. Cells cultured in absence of neurons had a complimentary gene profile with 20 statistically significant biological modules (blue histogram) including hallmark cholesterol homeostasis, hallmark TNFα signaling via NF-κB, leukocyte differentiation and regulation of IL-1β secretion.

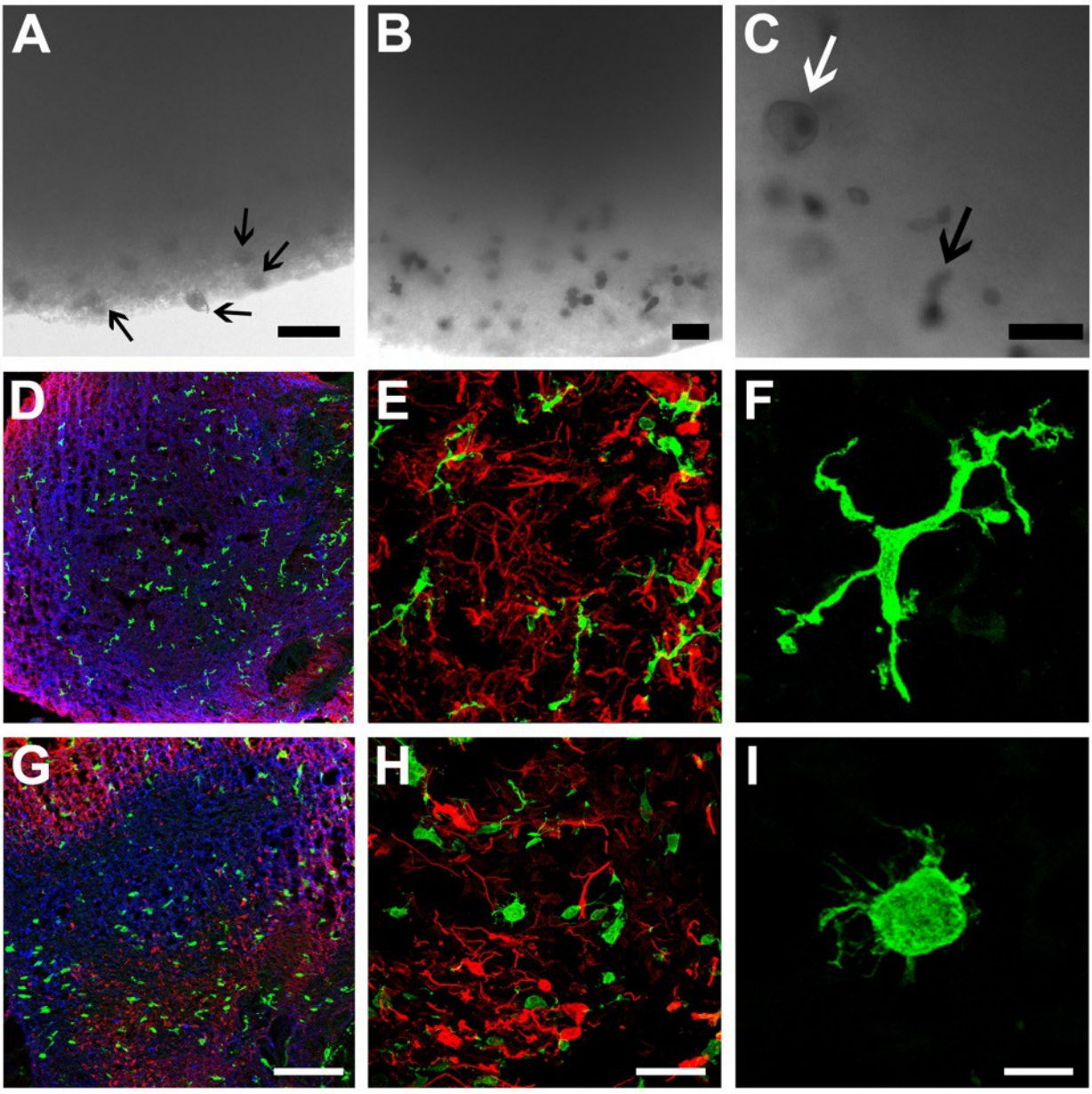

Figure 6. iMGLs respond to the neuronal environment in 3D brain organoid co-cultures (BORGs). iMGLs (5 x10^5 cells) were added to media containing a single BORG for 7 days. **(A)** Representative bright-field image of iMGLs detected in and near BORG after 3 days. iMGLs are found in and attached to BORG-media interface (arrows), but not free floating in the media, suggesting complete chemotaxis of iMGLs. **(B)** Representative image of iMGLs in outer and inner radius of BORG. **(C)** Embedded iMGLs exhibit macrophage-like morphology (white arrow) and extend processes (arrow) signifying ECM remodeling and surveillance respectively. Simultaneous assessment of

embedded iMGL morphology in uninjured **(D-F**) and injured **(G-I)** BORGs. **(D)** Immunohistochemical analysis of BORGs reveals iMGLs begin tiling evenly throughout the BORG and project ramified processes for surveillance of the environment. BORGs are representative of developing brains *in vitro* and contain neurons (β3-tubulin, blue) and astrocytes (GFAP, red), which self-organize into a cortical-like distribution, but lack microglia. iMGLs (IBA1, green). (**E-F**) Representative immunofluorescent images of iMGLs with extended processes within the 3D neuronal environment at higher magnification. **(G-I)** Representative images of iMGL morphology observed in injured BORG. **(H-I)** Round-bodied iMGLs reminiscent of amoeboid microglia are distributed in injured BORGs and closely resemble activated microglia, demonstrating that iMGLs respond appropriately to neuronal injury. Scale Bar (**A-C**) =50 μm in A-C, (**D,G**)= 200 μm (**E-H**)= 80 μm and (**F,I**) =15 μm.

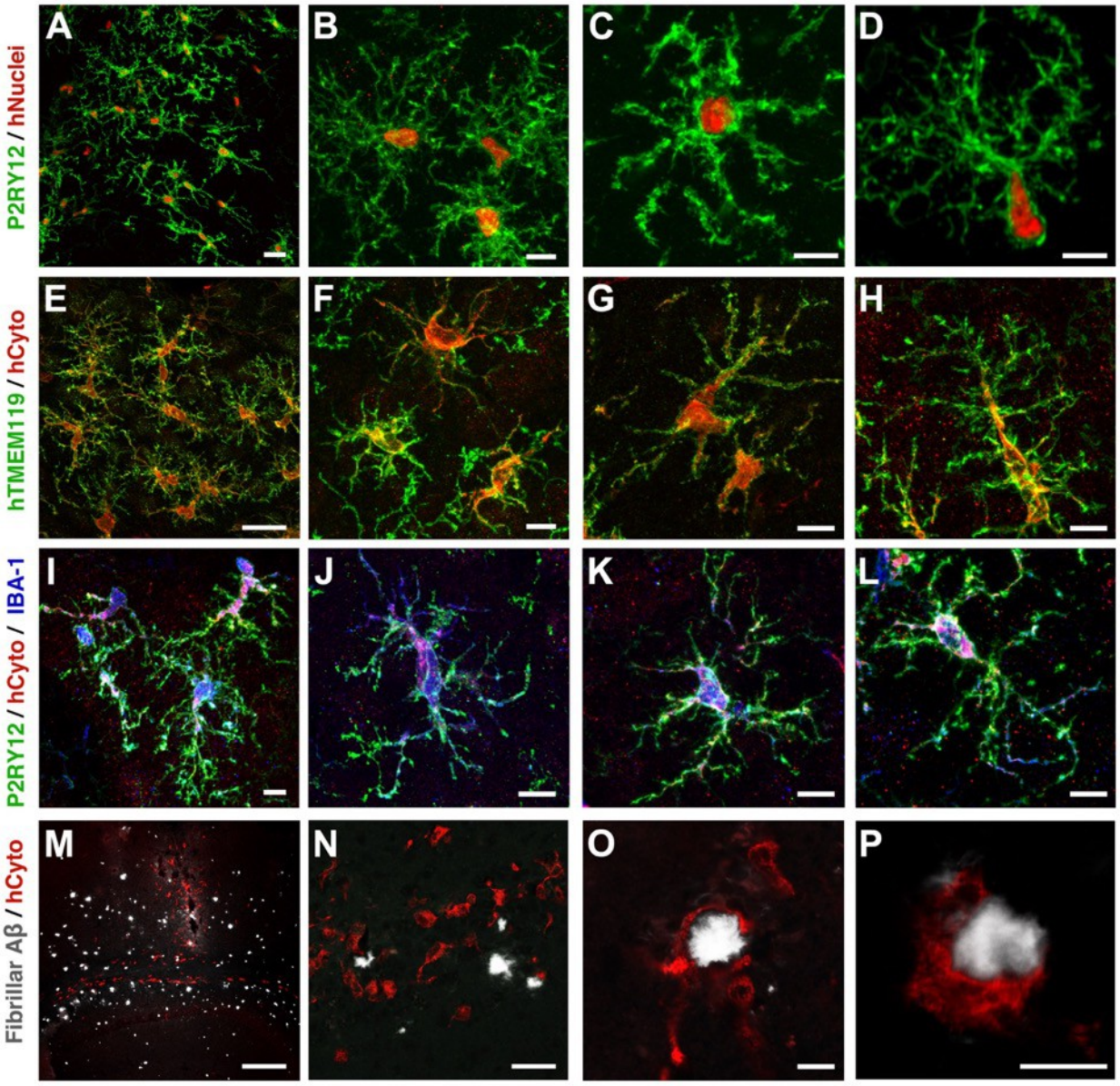

Figure 7. iMGLs transplanted into the brains of either wild-type or AD transplant competent mice are like brain microglia. Within the brains of xenotransplantation compatible mice, transplanted iMGLs are ramified and interacting with the neuronal environment. (**A-L**) After two months *in vivo,* iMGLs transplanted into mice display long-term viability with highly arborized processes resembling endogenous microglia found in the brain. (**A**) Transplanted iMGLs, labeled with P2ry12 (green; HPA HPA014518, Sigma/Atlas) and human nuclei (ku80, red), exhibit long-term viability in mice. (**B-D**) At higher magnification, P2ry12 is highly expressed in iMGL arborized processes, both

suggestive of homeostatic microglia surveying the brain environment. (**E-H**) Ramified iMGLs also express microglia-enriched TMEM119 recognized by a human-specific TMEM119 antibody (green; ab185333, Abcam, identified and validated in [Bennet et al, PNAS 2016]), and human cytoplasm maker SC121 (hCyto, red). (**I-L**) At higher magnification, representative iMGLs express P2ry12 (green), hCyto (red), and Iba1 (blue; ab5076, Abcam). (**M-P**) Human iMGLs (hCyto,red) transplanted into AD-immune-deficient mice (Marsh et al, PNAS 2016) interact with and phagocytose amyloid plaques (white). (**I-J**) Transplanted iMGLs extend projections and migrate to plaques. iMGLs fully encompass amyloid plaques (**O**) and begin to phagocytose amyloid (**P**). Scale bars; (**A,E,N**) = 30 μm, (**B-D, F-H, I-L, O,P**) = 10 μm, (**M**) = 300 μm. n=3 animals per study.

References

ABBAS, N., BEDNAR, I., MIX, E., MARIE, S., PATERSON, D., LJUNGBERG, A., MORRIS, C., WINBLAD, B., NORDBERG, A. & ZHU, J. 2002. Up-regulation of the inflammatory cytokines IFN-gamma and IL-12 and down-regulation of IL-4 in cerebral cortex regions of APP(SWE) transgenic mice. *J Neuroimmunol,* 126**,** 50-7.

ABDOLLAHI, A., LORD, K. A., HOFFMAN-LIEBERMANN, B. & LIEBERMANN, D. A. 1991. Interferon regulatory factor 1 is a myeloid differentiation primary response gene induced by interleukin 6 and leukemia inhibitory factor: role in growth inhibition. *Cell Growth Differ,* 2**,** 401-7.

ABUTBUL, S., SHAPIRO, J., SZAINGURTEN-SOLODKIN, I., LEVY, N., CARMY, Y., BARON, R., JUNG, S. & MONSONEGO, A. 2012. TGF-beta signaling through SMAD2/3 induces the quiescent microglial phenotype within the CNS environment. *Glia,* 60**,** 1160-71.

AGUZZI, A., BARRES, B. A. & BENNETT, M. L. 2013. Microglia: scapegoat, saboteur, or something else? *Science,* 339**,** 156-61.

ANDREASSON, K. I., BACHSTETTER, A. D., COLONNA, M., GINHOUX, F., HOLMES, C., LAMB, B., LANDRETH, G., LEE, D. C., LOW, D., LYNCH, M. A., MONSONEGO, A., O'BANION, M. K., PEKNY, M., PUSCHMANN, T., RUSSEK-BLUM, N., SANDUSKY, L. A., SELENICA, M. L., TAKATA, K., TEELING, J., TOWN, T. & VAN ELDIK, L. J. 2016. Targeting innate immunity for neurodegenerative disorders of the central nervous system. *J Neurochem,* 138**,** 653-93.

ASAI, H., IKEZU, S., TSUNODA, S., MEDALLA, M., LUEBKE, J., HAYDAR, T., WOLOZIN, B., BUTOVSKY, O., KUGLER, S. & IKEZU, T. 2015. Depletion of microglia and inhibition of exosome synthesis halt tau propagation. *Nat Neurosci,* 18**,** 1584-93.

BARON, R., BABCOCK, A. A., NEMIROVSKY, A., FINSEN, B. & MONSONEGO, A. 2014. Accelerated microglial pathology is associated with Abeta plaques in mouse models of Alzheimer's disease. *Aging Cell,* 13**,** 584-95.

BENNETT, M. L., BENNETT, F. C., LIDDELOW, S. A., AJAMI, B., ZAMANIAN, J. L., FERNHOFF, N. B., MULINYAWE, S. B., BOHLEN, C. J., ADIL, A., TUCKER, A., WEISSMAN, I. L., CHANG, E. F., LI, G., GRANT, G. A., HAYDEN GEPHART, M. G. & BARRES, B. A. 2016. New tools for studying microglia in the mouse and human CNS. *Proc Natl Acad Sci U S A,* 113**,** E1738-46.

BIBER, K., MOLLER, T., BODDEKE, E. & PRINZ, M. 2016. Central nervous system myeloid cells as drug targets: current status and translational challenges. *Nat Rev Drug Discov,* 15**,** 110-24.

BIBER, K., NEUMANN, H., INOUE, K. & BODDEKE, H. W. 2007. Neuronal 'On' and 'Off' signals control microglia. *Trends Neurosci,* 30**,** 596-602.

BLUM-DEGEN, D., MULLER, T., KUHN, W., GERLACH, M., PRZUNTEK, H. & RIEDERER, P. 1995. Interleukin-1 beta and interleukin-6 are elevated in the cerebrospinal fluid of Alzheimer's and de novo Parkinson's disease patients. *Neurosci Lett,* 202**,** 17-20.

BUTOVSKY, O., JEDRYCHOWSKI, M. P., MOORE, C. S., CIALIC, R., LANSER, A. J., GABRIELY, G., KOEGLSPERGER, T., DAKE, B., WU, P. M., DOYKAN, C. E., FANEK, Z., LIU, L., CHEN, Z., ROTHSTEIN, J. D., RANSOHOFF, R. M., GYGI, S. P., ANTEL, J. P. & WEINER, H. L. 2014. Identification of a unique TGF-beta-dependent molecular and functional signature in microglia. *Nat Neurosci,* 17**,** 131-43.

CHAN, W. Y., KOHSAKA, S. & REZAIE, P. 2007. The origin and cell lineage of microglia: new concepts. *Brain Res Rev,* 53**,** 344-54.

CHUNG, W. S., CLARKE, L. E., WANG, G. X., STAFFORD, B. K., SHER, A., CHAKRABORTY, C., JOUNG, J., FOO, L. C., THOMPSON, A., CHEN, C., SMITH, S. J. & BARRES, B. A. 2013. Astrocytes mediate synapse elimination through MEGF10 and MERTK pathways. *Nature,* 504**,** 394-400.

DE SIMONE, R., NITURAD, C. E., DE NUCCIO, C., AJMONE-CAT, M. A., VISENTIN, S. & MINGHETTI, L. 2010. TGF-beta and LPS modulate ADP-induced migration of microglial cells through P2Y1 and P2Y12 receptor expression. *J Neurochem,* 115**,** 450-9.

DOBIN, A., DAVIS, C. A., SCHLESINGER, F., DRENKOW, J., ZALESKI, C., JHA, S., BATUT, P., CHAISSON, M. & GINGERAS, T. R. 2013. STAR: ultrafast universal RNA-seq aligner. *Bioinformatics,* 29**,** 15-21.

DURAFOURT, B. A., MOORE, C. S., BLAIN, M. & ANTEL, J. P. 2013. Isolating, culturing, and polarizing primary human adult and fetal microglia. *Methods Mol Biol,* 1041**,** 199-211.

ERNY, D., HRABE DE ANGELIS, A. L., JAITIN, D., WIEGHOFER, P., STASZEWSKI, O., DAVID, E., KEREN-SHAUL, H., MAHLAKOIV, T., JAKOBSHAGEN, K., BUCH, T., SCHWIERZECK, V., UTERMOHLEN, O., CHUN, E., GARRETT, W. S., MCCOY, K. D., DIEFENBACH, A., STAEHELI, P., STECHER, B., AMIT, I. & PRINZ, M. 2015. Host microbiota constantly control maturation and function of microglia in the CNS. *Nat Neurosci,* 18**,** 965-77.

GINHOUX, F., GRETER, M., LEBOEUF, M., NANDI, S., SEE, P., GOKHAN, S., MEHLER, M. F., CONWAY, S. J., NG, L. G., STANLEY, E. R., SAMOKHVALOV, I. M. & MERAD, M. 2010. Fate mapping analysis reveals that adult microglia derive from primitive macrophages. *Science,* 330**,** 841-5.

GRABERT, K., MICHOEL, T., KARAVOLOS, M. H., CLOHISEY, S., BAILLIE, J. K., STEVENS, M. P., FREEMAN, T. C., SUMMERS, K. M. & MCCOLL, B. W. 2016. Microglial brain region-dependent diversity and selective regional sensitivities to aging. *Nat Neurosci,* 19**,** 504-16.

GRETER, M., LELIOS, I., PELCZAR, P., HOEFFEL, G., PRICE, J., LEBOEUF, M., KUNDIG, T. M., FREI, K., GINHOUX, F., MERAD, M. & BECHER, B. 2012. Stroma-derived interleukin-34 controls the development and maintenance of langerhans cells and the maintenance of microglia. *Immunity,* 37**,** 1050-60.

GUILLOT-SESTIER, M. V. & TOWN, T. 2013. Innate immunity in Alzheimer's disease: a complex affair. *CNS Neurol Disord Drug Targets,* 12**,** 593-607.

GYLYS, K. H., FEIN, J. A. & COLE, G. M. 2000. Quantitative characterization of crude synaptosomal fraction (P-2) components by flow cytometry. *J Neurosci Res,* 61**,** 186-92.

HANNA, R. N., CARLIN, L. M., HUBBELING, H. G., NACKIEWICZ, D., GREEN, A. M., PUNT, J. A., GEISSMANN, F. & HEDRICK, C. C. 2011. The transcription factor NR4A1 (Nur77) controls bone marrow differentiation and the survival of Ly6C- monocytes. *Nat Immunol,* 12**,** 778-85.

HAYNES, S. E., HOLLOPETER, G., YANG, G., KURPIUS, D., DAILEY, M. E., GAN, W. B. & JULIUS, D. 2006. The P2Y12 receptor regulates microglial activation by extracellular nucleotides. *Nat Neurosci,* 9**,** 1512-9.

HICKMAN, S. E., ALLISON, E. K. & EL KHOURY, J. 2008. Microglial dysfunction and defective beta-amyloid clearance pathways in aging Alzheimer's disease mice. *J Neurosci,* 28**,** 8354-60.

HICKMAN, S. E., KINGERY, N. D., OHSUMI, T. K., BOROWSKY, M. L., WANG, L. C., MEANS, T. K. & EL KHOURY, J. 2013. The microglial sensome revealed by direct RNA sequencing. *Nat Neurosci,* 16**,** 1896-905.

HONG, S., BEJA-GLASSER, V. F., NFONOYIM, B. M., FROUIN, A., LI, S., RAMAKRISHNAN, S., MERRY, K. M., SHI, Q., ROSENTHAL, A., BARRES, B. A., LEMERE, C. A., SELKOE, D. J. & STEVENS, B. 2016a. Complement and microglia mediate early synapse loss in Alzheimer mouse models. *Science,* 352**,** 712-6.

HONG, S., DISSING-OLESEN, L. & STEVENS, B. 2016b. New insights on the role of microglia in synaptic pruning in health and disease. *Curr Opin Neurobiol,* 36**,** 128-34.

KARCH, C. M., EZERSKIY, L. A., BERTELSEN, S., ALZHEIMER'S DISEASE GENETICS, C. & GOATE, A. M. 2016. Alzheimer's Disease Risk Polymorphisms Regulate Gene Expression in the ZCWPW1 and the CELF1 Loci. *PLoS One,* 11**,** e0148717.

KENNEDY, M., D'SOUZA, S. L., LYNCH-KATTMAN, M., SCHWANTZ, S. & KELLER, G. 2007. Development of the hemangioblast defines the onset of hematopoiesis in human ES cell differentiation cultures. *Blood,* 109**,** 2679-87.

KETTENMANN, H., HANISCH, U. K., NODA, M. & VERKHRATSKY, A. 2011. Physiology of microglia. *Physiol Rev,* 91**,** 461-553.
KIERDORF, K., ERNY, D., GOLDMANN, T., SANDER, V., SCHULZ, C., PERDIGUERO, E. G., WIEGHOFER, P., HEINRICH, A., RIEMKE, P., HOLSCHER, C., MULLER, D. N., LUCKOW, B., BROCKER, T., DEBOWSKI, K., FRITZ, G., OPDENAKKER, G., DIEFENBACH, A., BIBER, K., HEIKENWALDER, M., GEISSMANN, F., ROSENBAUER, F. & PRINZ, M. 2013. Microglia emerge from erythromyeloid precursors via Pu.1- and Irf8-dependent pathways. *Nat Neurosci,* 16**,** 273-80.
KOENIGSKNECHT-TALBOO, J. & LANDRETH, G. E. 2005. Microglial phagocytosis induced by fibrillar beta-amyloid and IgGs are differentially regulated by proinflammatory cytokines. *J Neurosci,* 25**,** 8240-9.
LANCASTER, M. A., RENNER, M., MARTIN, C. A., WENZEL, D., BICKNELL, L. S., HURLES, M. E., HOMFRAY, T., PENNINGER, J. M., JACKSON, A. P. & KNOBLICH, J. A. 2013. Cerebral organoids model human brain development and microcephaly. *Nature,* 501**,** 373-9.
LASAGNA-REEVES, C. A., CASTILLO-CARRANZA, D. L., SENGUPTA, U., SARMIENTO, J., TRONCOSO, J., JACKSON, G. R. & KAYED, R. 2012. Identification of oligomers at early stages of tau aggregation in Alzheimer's disease. *FASEB J,* 26**,** 1946-59.
LAVIN, Y., WINTER, D., BLECHER-GONEN, R., DAVID, E., KEREN-SHAUL, H., MERAD, M., JUNG, S. & AMIT, I. 2014. Tissue-resident macrophage enhancer landscapes are shaped by the local microenvironment. *Cell,* 159**,** 1312-26.
LI, B. & DEWEY, C. N. 2011. RSEM: accurate transcript quantification from RNA-Seq data with or without a reference genome. *BMC Bioinformatics,* 12**,** 323.
LINNARTZ-GERLACH, B., MATHEWS, M. & NEUMANN, H. 2014. Sensing the neuronal glycocalyx by glial sialic acid binding immunoglobulin-like lectins. *Neuroscience,* 275**,** 113-24.
LIU, Z., CONDELLO, C., SCHAIN, A., HARB, R. & GRUTZENDLER, J. 2010. CX3CR1 in microglia regulates brain amyloid deposition through selective protofibrillar amyloid-beta phagocytosis. *J Neurosci,* 30**,** 17091-101.
LOO, D. T., COPANI, A., PIKE, C. J., WHITTEMORE, E. R., WALENCEWICZ, A. J. & COTMAN, C. W. 1993. Apoptosis is induced by beta-amyloid in cultured central nervous system neurons. *Proc Natl Acad Sci U S A,* 90**,** 7951-5.
MARSH, S. E., ABUD, E. M., LAKATOS, A., KARIMZADEH, A., YEUNG, S. T., DAVTYAN, H., FOTE, G. M., LAU, L., WEINGER, J. G., LANE, T. E., INLAY, M. A., POON, W. W. & BLURTON-JONES, M. 2016. The adaptive immune system restrains Alzheimer's disease pathogenesis by modulating microglial function. *Proc Natl Acad Sci U S A,* 113**,** E1316-25.
MATCOVITCH-NATAN, O., WINTER, D. R., GILADI, A., VARGAS AGUILAR, S., SPINRAD, A., SARRAZIN, S., BEN-YEHUDA, H., DAVID, E., ZELADA GONZALEZ, F., PERRIN, P., KEREN-SHAUL, H., GURY, M., LARA-ASTAISO, D., THAISS, C. A., COHEN, M., BAHAR HALPERN, K., BARUCH, K., DECZKOWSKA, A., LORENZO-VIVAS, E., ITZKOVITZ, S., ELINAV, E., SIEWEKE, M. H., SCHWARTZ, M. & AMIT, I. 2016. Microglia development follows a stepwise program to regulate brain homeostasis. *Science,* 353**,** aad8670.

MILDNER, A., HUANG, H., RADKE, J., STENZEL, W. & PRILLER, J. 2017. P2Y12 receptor is expressed on human microglia under physiological conditions throughout development and is sensitive to neuroinflammatory diseases. *Glia,* 65**,** 375-387.

MOORE, C. S., ASE, A. R., KINSARA, A., RAO, V. T., MICHELL-ROBINSON, M., LEONG, S. Y., BUTOVSKY, O., LUDWIN, S. K., SEGUELA, P., BAR-OR, A. & ANTEL, J. P. 2015. P2Y12 expression and function in alternatively activated human microglia. *Neurol Neuroimmunol Neuroinflamm,* 2**,** e80.

MUFFAT, J., LI, Y., YUAN, B., MITALIPOVA, M., OMER, A., CORCORAN, S., BAKIASI, G., TSAI, L. H., AUBOURG, P., RANSOHOFF, R. M. & JAENISCH, R. 2016. Efficient derivation of microglia-like cells from human pluripotent stem cells. *Nat Med*.

PAOLICELLI, R. C., BOLASCO, G., PAGANI, F., MAGGI, L., SCIANNI, M., PANZANELLI, P., GIUSTETTO, M., FERREIRA, T. A., GUIDUCCI, E., DUMAS, L., RAGOZZINO, D. & GROSS, C. T. 2011. Synaptic pruning by microglia is necessary for normal brain development. *Science,* 333**,** 1456-8.

PATEL, N. S., PARIS, D., MATHURA, V., QUADROS, A. N., CRAWFORD, F. C. & MULLAN, M. J. 2005. Inflammatory cytokine levels correlate with amyloid load in transgenic mouse models of Alzheimer's disease. *J Neuroinflammation,* 2**,** 9.

PRINZ, M. & PRILLER, J. 2014. Microglia and brain macrophages in the molecular age: from origin to neuropsychiatric disease. *Nat Rev Neurosci,* 15**,** 300-12.

PRINZ, M., PRILLER, J., SISODIA, S. S. & RANSOHOFF, R. M. 2011. Heterogeneity of CNS myeloid cells and their roles in neurodegeneration. *Nat Neurosci,* 14**,** 1227-35.

REZAIE, P. & MALE, D. 1999. Colonisation of the developing human brain and spinal cord by microglia: a review. *Microsc Res Tech,* 45**,** 359-82.

ROBINSON, M. D., MCCARTHY, D. J. & SMYTH, G. K. 2010. edgeR: a Bioconductor package for differential expression analysis of digital gene expression data. *Bioinformatics,* 26**,** 139-40.

RONGVAUX, A., WILLINGER, T., MARTINEK, J., STROWIG, T., GEARTY, S. V., TEICHMANN, L. L., SAITO, Y., MARCHES, F., HALENE, S., PALUCKA, A. K., MANZ, M. G. & FLAVELL, R. A. 2014. Development and function of human innate immune cells in a humanized mouse model. *Nat Biotechnol,* 32**,** 364-72.

RUSTENHOVEN, J., PARK, T. I., SCHWEDER, P., SCOTTER, J., CORREIA, J., SMITH, A. M., GIBBONS, H. M., OLDFIELD, R. L., BERGIN, P. S., MEE, E. W., FAULL, R. L., CURTIS, M. A., SCOTT GRAHAM, E. & DRAGUNOW, M. 2016. Isolation of highly enriched primary human microglia for functional studies. *Sci Rep,* 6**,** 19371.

SCHILLING, T., NITSCH, R., HEINEMANN, U., HAAS, D. & EDER, C. 2001. Astrocyte-released cytokines induce ramification and outward K+ channel expression in microglia via distinct signalling pathways. *Eur J Neurosci,* 14**,** 463-73.

SCHULZ, C., GOMEZ PERDIGUERO, E., CHORRO, L., SZABO-ROGERS, H., CAGNARD, N., KIERDORF, K., PRINZ, M., WU, B., JACOBSEN, S. E., POLLARD, J. W., FRAMPTON, J., LIU, K. J. & GEISSMANN, F. 2012. A lineage of myeloid cells independent of Myb and hematopoietic stem cells. *Science,* 336**,** 86-90.

SHULMAN, J. M., IMBOYWA, S., GIAGTZOGLOU, N., POWERS, M. P., HU, Y., DEVENPORT, D., CHIPENDO, P., CHIBNIK, L. B., DIAMOND, A., PERRIMON, N., BROWN, N. H., DE JAGER, P. L. & FEANY, M. B. 2014. Functional screening in Drosophila identifies Alzheimer's disease susceptibility genes and implicates Tau-mediated mechanisms. *Hum Mol Genet,* 23**,** 870-7.

SIRKIS, D. W., BONHAM, L. W., APARICIO, R. E., GEIER, E. G., RAMOS, E. M., WANG, Q., KARYDAS, A., MILLER, Z. A., MILLER, B. L., COPPOLA, G. & YOKOYAMA, J. S. 2016. Rare TREM2 variants associated with Alzheimer's disease display reduced cell surface expression. *Acta Neuropathol Commun,* 4**,** 98.

STALDER, A. K., ERMINI, F., BONDOLFI, L., KRENGER, W., BURBACH, G. J., DELLER, T., COOMARASWAMY, J., STAUFENBIEL, M., LANDMANN, R. & JUCKER, M. 2005. Invasion of hematopoietic cells into the brain of amyloid precursor protein transgenic mice. *J Neurosci,* 25**,** 11125-32.

STEPHAN, A. H., BARRES, B. A. & STEVENS, B. 2012. The complement system: an unexpected role in synaptic pruning during development and disease. *Annu Rev Neurosci,* 35**,** 369-89.

STURGEON, C. M., DITADI, A., AWONG, G., KENNEDY, M. & KELLER, G. 2014. Wnt signaling controls the specification of definitive and primitive hematopoiesis from human pluripotent stem cells. *Nat Biotechnol,* 32**,** 554-61.

VILLEGAS-LLERENA, C., PHILLIPS, A., GARCIA-REITBOECK, P., HARDY, J. & POCOCK, J. M. 2015. Microglial genes regulating neuroinflammation in the progression of Alzheimer's disease. *Curr Opin Neurobiol,* 36**,** 74-81.

WANG, W. Y., TAN, M. S., YU, J. T. & TAN, L. 2015. Role of pro-inflammatory cytokines released from microglia in Alzheimer's disease. *Ann Transl Med,* 3**,** 136.

WANG, Y., SZRETTER, K. J., VERMI, W., GILFILLAN, S., ROSSINI, C., CELLA, M., BARROW, A. D., DIAMOND, M. S. & COLONNA, M. 2012. IL-34 is a tissue-restricted ligand of CSF1R required for the development of Langerhans cells and microglia. *Nat Immunol,* 13**,** 753-60.

YAMASAKI, R., LU, H., BUTOVSKY, O., OHNO, N., RIETSCH, A. M., CIALIC, R., WU, P. M., DOYKAN, C. E., LIN, J., COTLEUR, A. C., KIDD, G., ZORLU, M. M., SUN, N., HU, W., LIU, L., LEE, J. C., TAYLOR, S. E., UEHLEIN, L., DIXON, D., GU, J., FLORUTA, C. M., ZHU, M., CHARO, I. F., WEINER, H. L. & RANSOHOFF, R. M. 2014. Differential roles of microglia and monocytes in the inflamed central nervous system. *J Exp Med,* 211**,** 1533-49.

ZHANG, Y., CHEN, K., SLOAN, S. A., BENNETT, M. L., SCHOLZE, A. R., O'KEEFFE, S., PHATNANI, H. P., GUARNIERI, P., CANEDA, C., RUDERISCH, N., DENG, S., LIDDELOW, S. A., ZHANG, C., DANEMAN, R., MANIATIS, T., BARRES, B. A. & WU, J. Q. 2014. An RNA-sequencing transcriptome and splicing database of glia, neurons, and vascular cells of the cerebral cortex. *J Neurosci,* 34**,** 11929-47.

Supplemental Figure and Table Legends

Figure S1

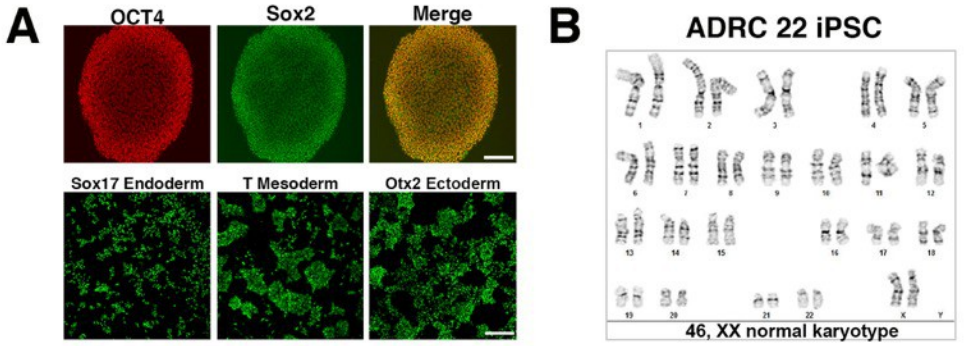

C

iPSC ID	Source	iPSC Karyotype	Sex	Pluritest Score	Pluritest (pass vs. fail)	Novelty Score	Novelty (pass vs. fail)
ADRC iPS 2	Fibroblast	46 XY normal	Male	19.29	Pass	1.511	Pass
ADRC iPS 4	Fibroblast	46 XY normal	Male	23.09	Pass	1.449	Pass
ADRC iPS 5	Fibroblast	46 XX normal	Female	21.85	Pass	1.409	Pass
ADRC iPS 12	PBMC	46 XY normal	Male	26.45	Pass	1.519	Pass
ADRC iPS 14	Fibroblast	46 XY normal	Male	26.85	Pass	1.418	Pass
ADRC iPS 20	Fibroblast	46 XX normal	Female	27.19	Pass	1.376	Pass
ADRC iPS 22	Fibroblast	46 XX normal	Female	22.82	Pass	1.404	Pass
ADRC iPS 76	PBMC	46 XY normal	Male	21.37	Pass	1.433	Pass
ADRC iPS 85	Fibroblast	46 XY normal	Male	33.73	Pass	1.325	Pass
ADRC iPS 86	Fibroblast	46 XX normal	Female	32.70	Pass	1.276	Pass

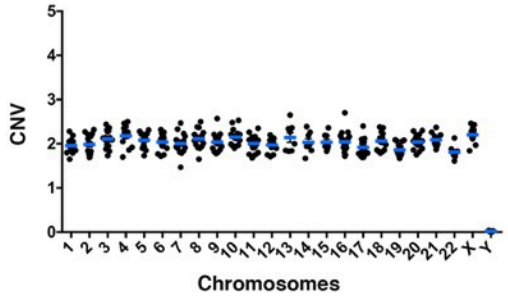

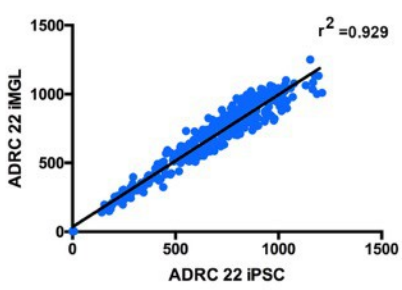

E

ID	Karyotype	Sex	Aneuploidy
iPSC			
ADRC iPS 5	46 XX normal	Female	No
ADRC iPS 14	46 XY normal	Male	No
ADRC iPS 22	46 XX normal	Female	No
ADRC iPS 76	46 XY normal	Male	No
ADRC iPS 76 Replicate	46 XY normal	Male	No
CDI iHPC	46 XY normal	Male	No
iMGL			
ADRC iMGL 5	46 XX normal	Female	No
ADRC iMGL 14	46 XY normal	Male	No
ADRC iMGL 22	46 XX normal	Female	No
ADRC iMGL 76	46 XY normal	Male	No
ADRC iMGL 76 Replicate	46 XY normal	Male	No
CDI iMGL	46 XY normal	Male	No

Figure S1, **related to Figure 1. Genomic stability of iPSCs and iMGLs.** (**A**) Top: Representative fluorescent images of iPSCs expressing the pluripotent markers OCT4 (red) and SOX2 (green). Scale bar =300 μm. Bottom: Functional validation of pluripotency in iPSCs. Representative fluorescent images of iPSCs differentiated to endoderm, mesoderm and ectoderm and stained for Sox17, T (Brachyury), and Otx2 respectively to validate differentiation potential. Scale bar =200 μm. (**B-C**) Karyotype and Pluritest scores indicate all iPS lines generated using Sendai virus and used in this study were karyotopically normal and pluripotent. The Pluritest is a microarray-based assessment of pluripotency based on iPS whole transcriptome analysis referenced to a library of functionally validated iPSCs (Muller, F.J. et al. 2011). (**D-E**) Maintenance of genomic stability over the course of iMGL differentiation using pluripotent iPS or commercial hematopoietic progenitors. CNV assessment of differentiated iMGLs reveals genomic stability is maintained over the course of differentiation. (**D**) Representative Nanostring nCounterKaryotype results demonstrate that microglia derived from ADRC iPS line 22 do not inherit extrachromosomal DNA over the course of differentiation. (**E**) Quantification of the 338 probe sets across all 24 chromosomes do not reveal any chromosomal abnormalities (n=6). (**F**) Representative analysis of iMGL derived from its iPSC show strong CNV correlation (r^2=0.929) showing sensitivity of assay and genomic stability of derived iMGLs.

Figure S2

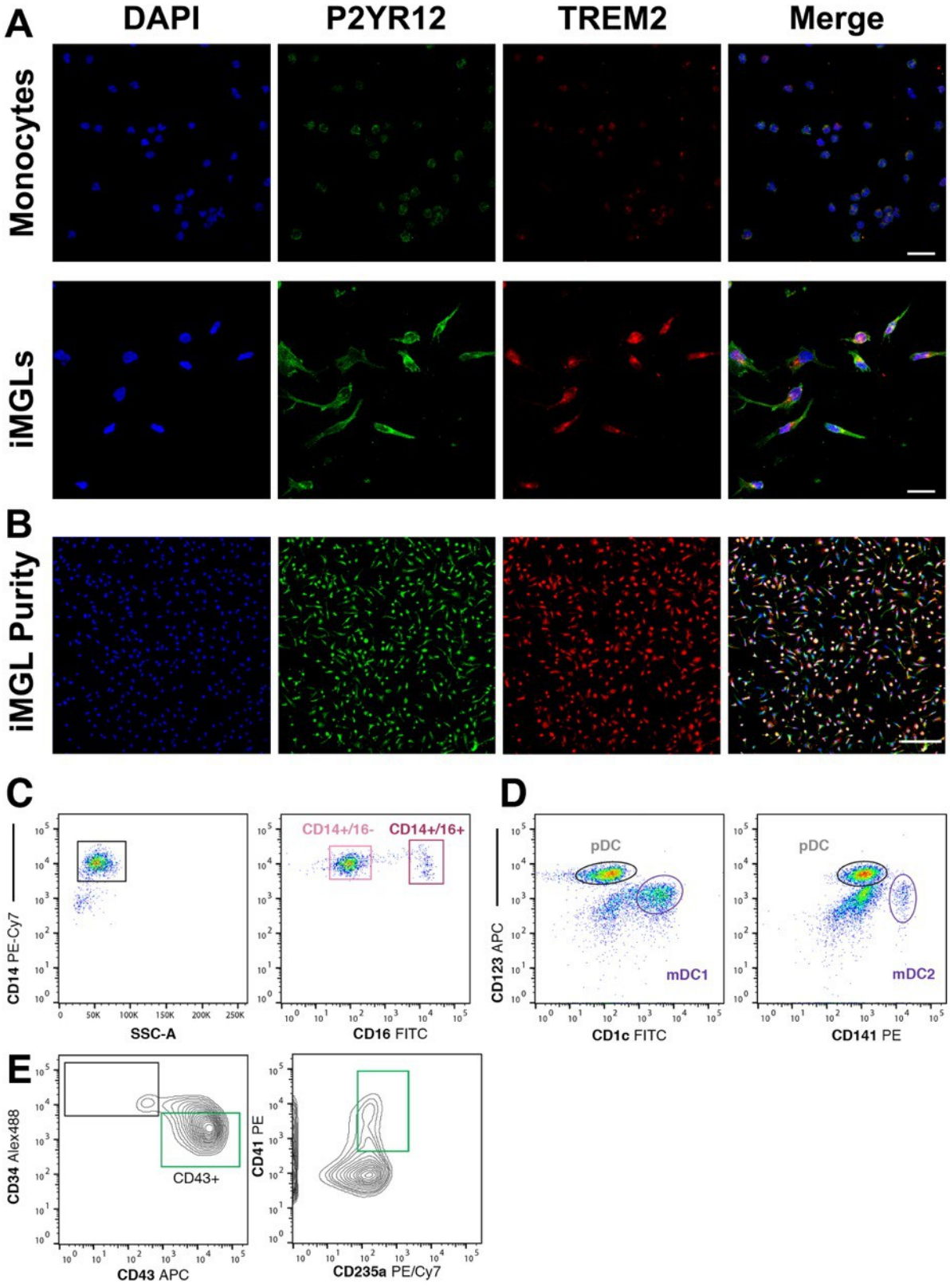
A
DAPI
P2YR12
TREM2
Merge
Monocytes
iMGLs
B
iMGL Purity
C
CD14 PE-Cy7
SSC-A
CD14+/16-
CD14+/16+
CD16 FITC
D
pDC
mDC1
mDC2
CD123 APC
CD1c FITC
CD141 PE
E
CD34 Alex488
CD43+
CD43 APC
CD41 PE
CD235a PE/Cy7

Figure S2, related to Figure 1 and Figure 2. Assessment of iMGL purity by P2RY12/TREM2 co-localization and flow cytometry characterization of monocytes, dendritic cells and commercial iHPCs. (**A**) Specificity assessment of rabbit anti-human P2RY12 (HPA014518, also recently validated by (Mildner et al., 2017), and goat anti-human TREM2 (R&D, AF1828) in human monocytes and iMGLs. scale bar = 20 μm (**B**) Representative immunofluorescent images (from 5 representative lines) of iMGL purity by P2RY12/TREM2/DAPI co-localization. scale bar = 100μm (**C**) Human $CD14^{+}/CD16^{-}$ monocytes and $CD14^{+}/CD16^{+}$ inflammatory monocytes, CD14M and CD16M respectively, were isolated from young healthy human blood (18-39 y.o.) by FACs. Cells were first gated on viability (not shown), then CD14 to avoid contaminating leukocytes, and finally sorted according to CD16 expression and collected for RNA. (**D**) Human myeloid dendritic cells (Blood DCs) were isolated from young healthy human blood (18-39 y.o.) using untouched myeloid DC enrichment kit followed by FACs. To avoid plasmacytoid DC contamination, DCs were stained for CD123, and myeloid DC subtypes CD1c, and C141 were collected for RNA. (**E**) A commercial iPSC-HPC source ($CD43^{+}/235a^{+}/CD41^{+}$) cells were identified and used to compare to in-house HPC differentiation and further iMGL differentiation.

Figure S3

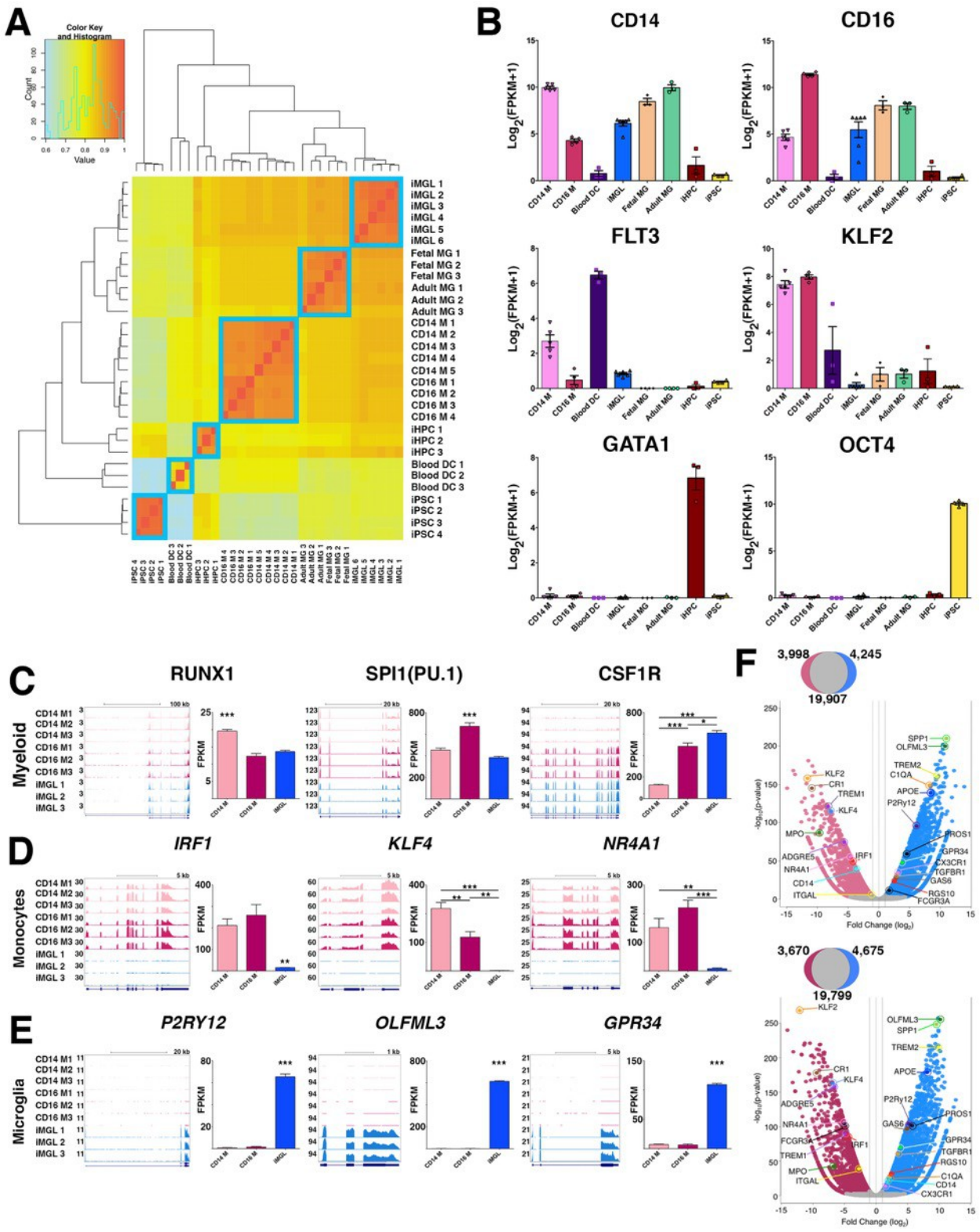
A
Color Key and Histogram
Count
Value
iMGL 1
iMGL 2
iMGL 3
iMGL 4
iMGL 5
iMGL 6
Fetal MG 1
Fetal MG 2
Fetal MG 3
Adult MG 1
Adult MG 2
Adult MG 3
CD14 M 1
CD14 M 2
CD14 M 3
CD14 M 4
CD14 M 5
CD16 M 1
CD16 M 2
CD16 M 3
CD16 M 4
iHPC 1
iHPC 2
iHPC 3
Blood DC 1
Blood DC 2
Blood DC 3
iPSC 1
iPSC 2
iPSC 3
iPSC 4
B
CD14
CD16
FLT3
KLF2
GATA1
OCT4
Log2(FPKM+1)
CD14 M
CD16 M
Blood DC
iMGL
Fetal MG
Adult MG
iHPC
iPSC
C
RUNX1
SPI1(PU.1)
CSF1R
Myeloid
FPKM
D
IRF1
KLF4
NR4A1
Monocytes
E
P2RY12
OLFML3
GPR34
Microglia
F
3,998
4,245
19,907
SPP1
OLFML3
TREM2
C1QA
APOE
P2Ry12
KLF2
CR1
TREM1
KLF4
MPO
ADGRE5
IRF1
NR4A1
CD14
ITGAL
P2RY12
GPR34
CX3CR1
TGFBR1
GAS6
RGS10
FCGR3A
-log10(p-value)
Fold Change (log2)
3,670
4,675
19,799
FCGR3A
TREM1

Figure S3, related to Figure 2. Correlational Matrix of biological samples used in RNA-sequencing and iMGL gene example genes. (**A**) Spearmen correlational matrix of biological samples used in RNA-sequencing highlights strong intra-group correlation. iMGLs correlate well with Fetal and Adult MGs suggesting strong gene expression similarity between samples. (**B**) Histograms of key genes found across different samples. CD14 and FCGR3A (also known as CD16) expressed in all myeloid cells including microglia, although enriched in CD14 M and CD16 M, respectively. As expected, FLT3 is highly expressed in Blood DCs and not in other cells and is barely detected in all three microglia groups. The monocyte/macrophage-specific transcription factor KLF2 was enriched in only CD14 M and CD16 M. Whereas GATA1 and OCT4 were only detected in iHPCs and iPSCs, respectively. (**C-F**) RNA-sequencing expression profile of iMGL reveals they are unique from CD14M^{-} and CD16M and highly express microglial genes. (**C-E**) RNA-seq coverage maps and gene FPKM values in CD14 M, CD16 M, and iMGL for (**C**) for the myeloid genes RUNX1, PU.1, and CSF1R (**D**) monocyte-enriched genes IRF1, KLF4, and NR4A1 and (**E**) microglial-enriched genes P2RY12, OLFML3, and GPR34 in iMGL. For all RNA coverage maps, the y-axis represents Reads Per Million (RPM) scaled accordingly for all samples. Histogram comparisons using FPKM values for all genes are shown as the mean± s.e.m. Biological replicates for CD14 M (n=5), CD16 (n=4), and iMGL (n=6) are included for comparison by one-way ANOVA followed by Turkey's multiple-comparison post-hoc test. **p<0.001, ***p<0.0001. (F) Representative volcano plots of differentially expressed genes (p-value < 0.001, two-fold change) in iMGL (blue), CD14 M (light pink), and non-significant (grey). Key genes are both colored and labeled uniquely. Fold change (log_2) and $–log_{10}$(p-value) indicate the x and y-axis respectively. Grey dashed vertical lines indicate a two-fold change in gene expression. Venn diagrams indicate total number of differentially expressed genes for each condition.

Figure S4

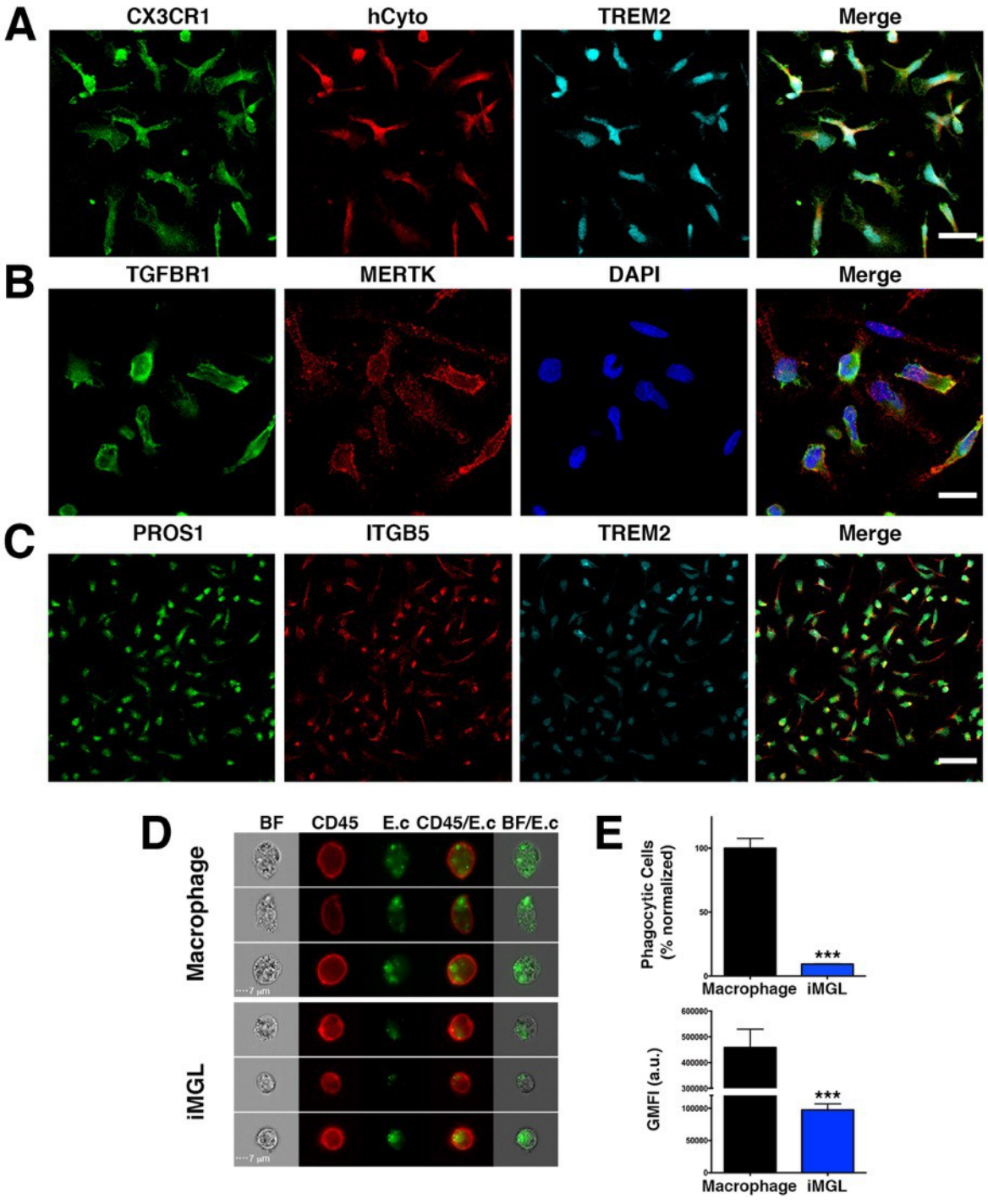
A
CX3CR1
hCyto
TREM2
Merge
B
TGFBR1
MERTK
DAPI
Merge
C
PROS1
ITGB5
TREM2
Merge
D
BF
CD45
E.c
CD45/E.c
BF/E.c
Macrophage
iMGL
7 μm
E
Phagocytic Cells (% normalized)
100
50
0
***
Macrophage
iMGL
GMFI (a.u.)
600000
500000
400000
300000
100000
50000
0
***
Macrophage
iMGL

Figure S4, related to Figure 3. iMGLS are positive for microglia surface proteins and perform phagocytosis of *E. coli* particles. Representative immunofluorescent images of iMGL expressing microglial markers (**A**) CX3CR1 (green), hCyto (human cytoplasm marker, SC121; red), TREM2 (cyan). scale bar = 20 μm (**B**) Co-localization of TGFBR1(green), MERTK (red), nuclei (DAPI, blue) scale bar = 20 μm. (**C**) PROS1 (green), ITGB5 (red), TREM2 (cyan). scale bar = 100 μm (**D-E**) Assessment of phagocytosis of pHrodo-labeled *E. coli* (E.c; green) (**D-E**) in human monocyte-derived macrophages (black) and iMGLs (blue). (**D**) Representative bright field and immunofluorescent images captured by Amnis Imagestream flow cytometer visualizing phagocytosis of E.c within macrophages (top) and iMGL (bottom). (**E**) Quantification of percent phagocytic cells (top) reveals that iMGLs (blue) phagocytose E.c almost 10-fold less frequently than macrophages (black) as expected. (**B:** bottom) The amount of E.c internalized (by GMFI) within phagocytic cells further illustrates the greater phagocytic capacity of macrophages compared to iMGLs. Student's T-test,*** $p<0.001$, n=3/group.

Figure S5

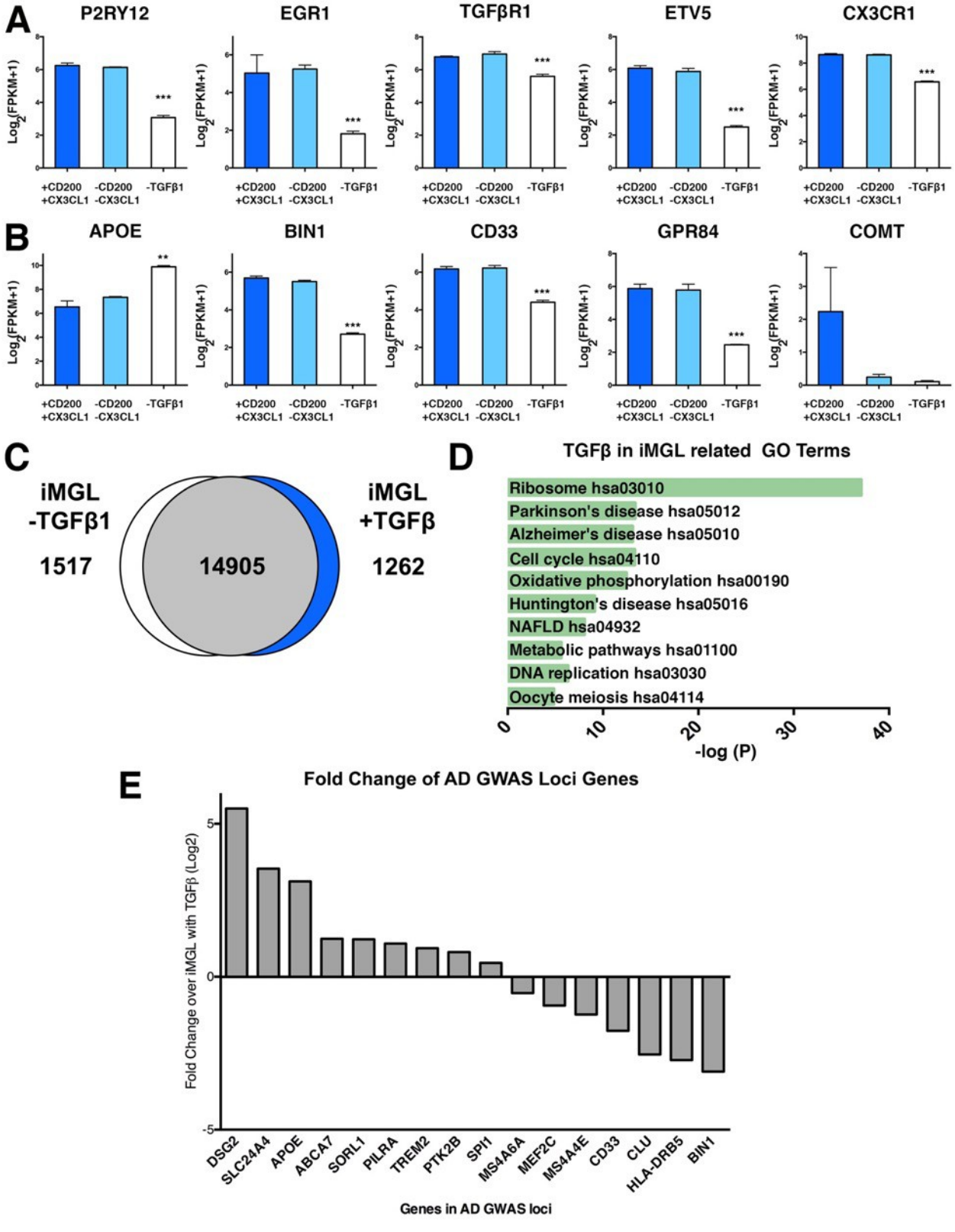
A
P2RY12
EGR1
TGFβR1
ETV5
CX3CR1
B
APOE
BIN1
CD33
GPR84
COMT
Log2(FPKM+1)
+CD200 +CX3CL1
-CD200 -CX3CL1
-TGFβ1
C
iMGL -TGFβ1
1517
14905
iMGL +TGFβ
1262
D
TGFβ in iMGL related GO Terms
Ribosome hsa03010
Parkinson's disease hsa05012
Alzheimer's disease hsa05010
Cell cycle hsa04110
Oxidative phosphorylation hsa00190
Huntington's disease hsa05016
NAFLD hsa04932
Metabolic pathways hsa01100
DNA replication hsa03030
Oocyte meiosis hsa04114
-log (P)
E
Fold Change of AD GWAS Loci Genes
Fold Change over iMGL with TGFβ (Log2)
DSG2
SLC24A4
APOE
ABCA7
SORL1
PILRA
TREM2
PTK2B
SPI1
MS4A6A
MEF2C
MS4A4E
CD33
CLU
HLA-DRB5
BIN1
Genes in AD GWAS loci

Figure S5, related to Figure 2 and 4. TGFβ-1, CX3CL1, CD200 and their impact on key microglial genes are associated with modulating neuronal function and environment. (**A-B**) TGFβ1 maintains core microglial genes. Withdrawal of TGFβ1 for 24 h (white) bars strongly influences microglial transcriptome. In agreement with mouse studies in vivo (Butovsky, et al, 2014), TGFβ removal reduces expression of key microglia genes including surface receptors P2RY12, TGFβR1, and CX3CR1, while also reducing expression of microglia transcription factors EGR1 and ETV5. AD-associated pathway genes such as BIN1, CD33, and APOE are also influenced by the lack of TGFβ. Removal of CX3CL1 and CD200, does not change core microglia identity, but impacts state by influencing homeostatic gene expression such as, COMT, and APOE (*B*). (**C**) Differential gene expression analysis reveals that presence of TGFβ increases expression of 1262 genes in iMGLs, while lack of TGFβ reduces expression, further supporting previous work highlighting the role of TGFB in microglia development, gene signature, and function. (**D**) KEGG pathway analysis highlights that microglial-core genes, elevated with TGFβ, modulate pathways in CNS disease including. Statistics reflect one-way ANOVA followed by Dunnett's multiple-comparison post-*hoc* test. * $p<0.05$**$p<0.001$, ***$p<0.0001$.

Figure S6

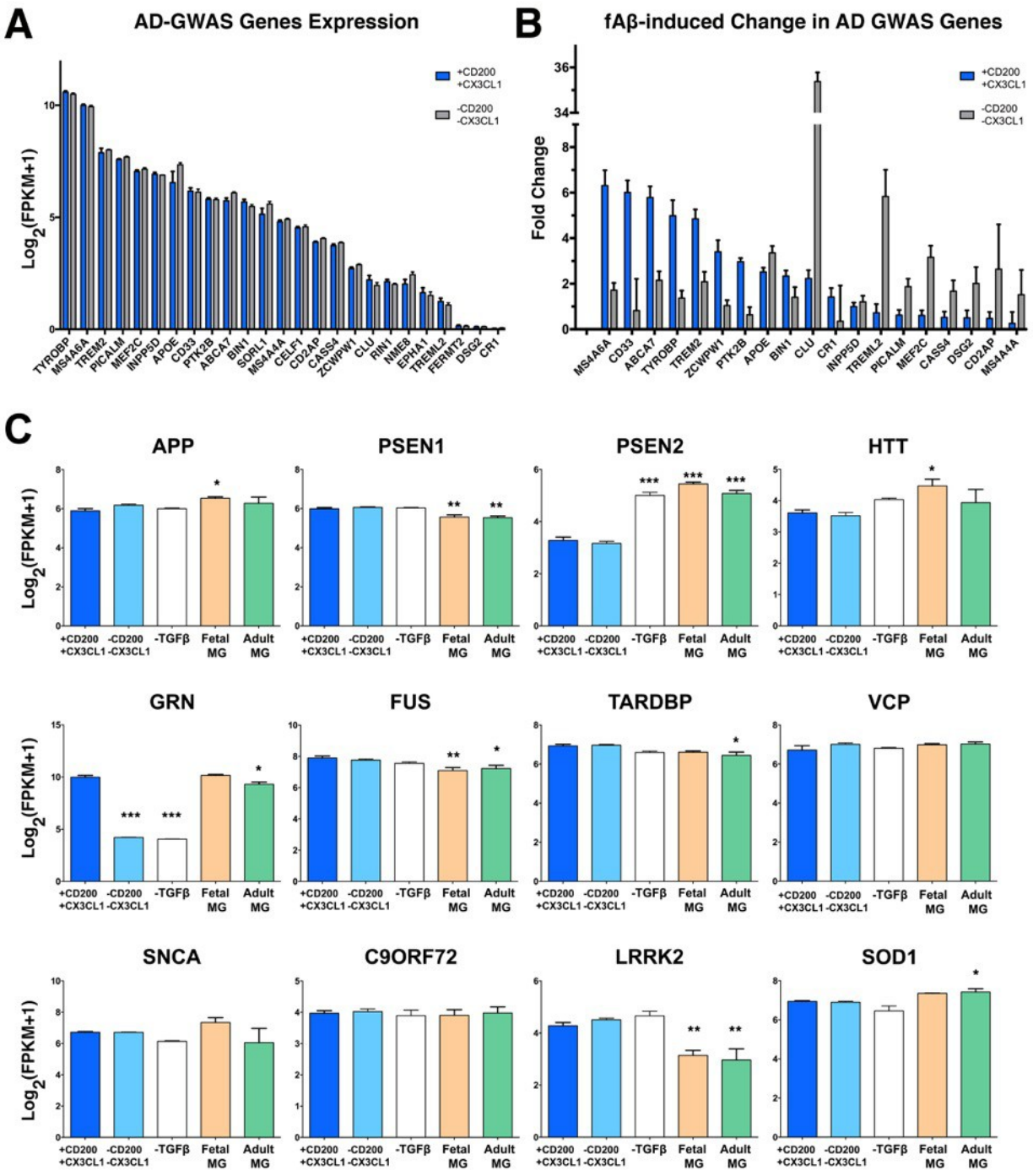

Figure S6, related to Figures 4 and 5. Microglia AD-GWAS and CNS-disease related genes can be studied using iMGLs. (**A-B**) iMGL AD-related GWAS genes respond to fAβ differentially if primed with or without CD200 and CX3CL1. iMGL exposure to CNS factors, CD200 and CX3CL1, "primes" their response fAβ by increasing expression of genes with functions implicated to modulate microglia inflammation and function in AD, like CD33, ABCA7, TYROBP, and TREM2. Stimulation with fAβ of iMGLs not exposed to CD200 or CX3CL1 results in increase expression of AD GWAS -related genes CLU and APOE, genes involved in response to misfolded proteins as well as survival and homeostasis. (**C**) Major neurodegenerative related genes, APP (AD), SCNA (PD) and HTT (HD), are expressed in iMGLs and primary microglia. iMGLs also express genes linked to Amylotrophic Lateral

Sclerosis (ALS), Frontaltemporal Dementia (FTD), and Dementia with Lewy Bodies (DLB) and implicate microglia dysfunction**.** Bar graphs of genes implicated in neurodegenerative diseases that are detected in iMGL similarly to Fetal and Adult MG, and expressed Log_2 (FPKM +1) presented as mean ± SEM. Like isolated human primary microglia, iMGLs express Valosin Containing Protein (VCP), FUS binding protein (FUS), proganulin (GRN), TDP-43 (TARDBP), LRRK2, and Superoxide Dismutase (SOD). Recent literature implicates microglia dysfunction related to mutations or loss of function of these genes playing a role in the pathogenesis of ALS (SOD1, TARDBP, FUS), FTD (VCP, GRN, TARDBP), PD (LRRK2, SNCA), and DLB (SNCA), suggesting the utility of iMGLs in studying the underlying mechanism of these genes in these neurological diseases. Statistics reflect one-way ANOVA followed by Turkey's multiple-comparison *post-hoc* test. * $p<0.05$**$p<0.001$, ***$p<0.0001$.

Figure S7

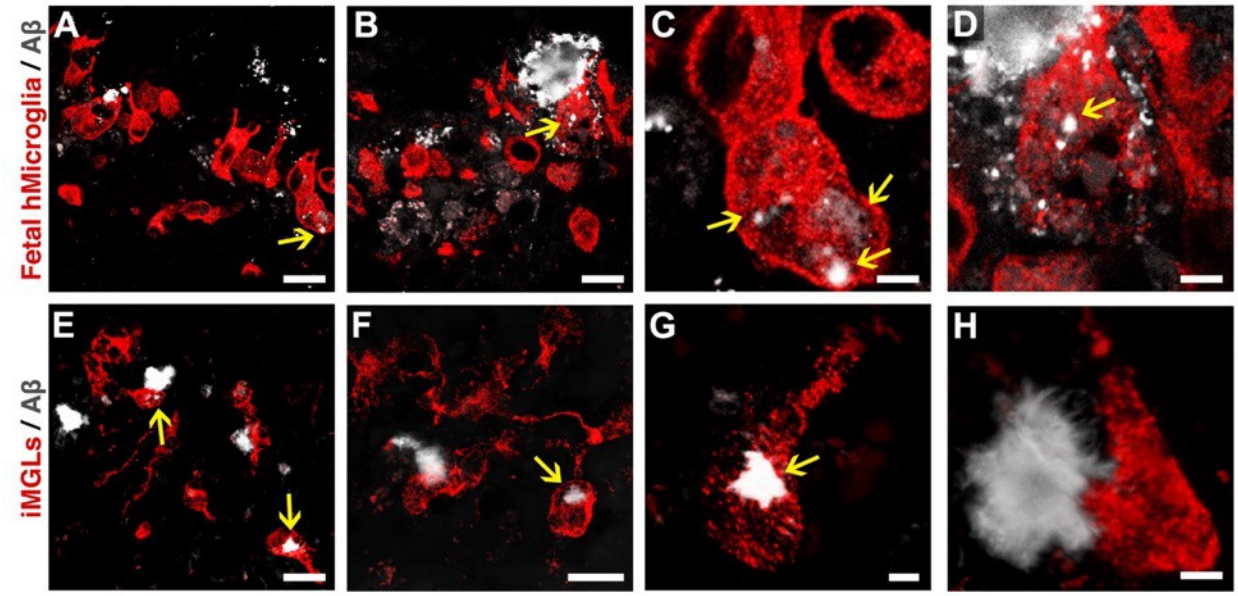

Figure S7, related to Figure 7. iPS-derived microglial cells engraft and phagocytose Aβ like human fetal microglia. (**A-D**) Human fetal microglia (hCyto, red) were transplanted into immune deficient AD mouse model, Rag5xfAD (Marsh et al, 2016), and respond to beta-amyloid plaques. Fetal microglia are observed surrounding plaques (**C**), and phagocytosing Aβ (**C-D**). (**E-H**) Like fetal microglia, iMGLs (hCyto, red) surround and phagocytose beta-amyloid plaques. Scale bars (**A,B,E,F**) = 20 μm, (**C,D,H,G**) 5 μm.

Table 1, related to Figure 2. Statistical adjusted *p*-values for 12 genes in histograms. one -way ANOVA followed by Tukey's *post-hoc* test.

Table S1 **Table 2, related to Figure 3.** Elisa cytokine values (pg/ml) from conditioned media of iMGLs stimulated by IFNγ, [illegible] ANOVA followed by Dunnett's *post-hoc* test. Adjusted *p*-values for multiple comparisons are reported.

fold change greater than 2. Results presented as mean ± standard error. (n=6 per group). Two-way ANOVA followed by Sidak's *post-hoc* test. Adjusted *p*-values for multiple comparisons.

Table 5, related to Figure 2. Gene ontology terms enriched in Fetal MG vs Adult MG and iMGL.

	GENES					
COMPARISONS	**P2RY12**	**GPR34**	**CABLES1**	**BHLHE41**	**TREM2**	**OLFML3**
CD14+ M VS. CD16+ M	0.7965	> 0.9999	> 0.9999	> 0.9999	0.9987	0.9871
CD14+ M VS. BLOOD DC	0.7534	0.0065	0.5006	> 0.9999	0.0405	> 0.9999
CD14+ M VS. IMGL	< 0.0001	< 0.0001	< 0.0001	0.0064	< 0.0001	< 0.0001
CD14+ M VS. FETAL MG	< 0.0001	< 0.0001	< 0.0001	< 0.0001	< 0.0001	< 0.0001
CD14+ M VS. ADULT MG	< 0.0001	< 0.0001	< 0.0001	< 0.0001	< 0.0001	< 0.0001
CD16+ M VS. BLOOD DC	0.2047	0.0129	0.6603	> 0.9999	0.8586	0.9976
CD16+ M VS. IMGL	< 0.0001	< 0.0001	< 0.0001	0.0111	< 0.0001	< 0.0001
CD16+ M VS. FETAL MG	0.0004	< 0.0001	< 0.0001	< 0.0001	< 0.0001	< 0.0001
CD16+ M VS. ADULT MG	0.0002	< 0.0001	< 0.0001	< 0.0001	< 0.0001	< 0.0001
BLOOD DC VS. IMGL	< 0.0001	< 0.0001	< 0.0001	0.0256	< 0.0001	< 0.0001
BLOOD DC VS. FETAL MG	< 0.0001	< 0.0001	< 0.0001	0.0001	< 0.0001	< 0.0001
BLOOD DC VS. ADULT MG	< 0.0001	< 0.0001	< 0.0001	< 0.0001	< 0.0001	< 0.0001
IMGL VS. FETAL MG	< 0.0001	> 0.9999	0.9483	0.0256	0.0633	< 0.0001
IMGL VS. ADULT MG	< 0.0001	0.8258	0.3015	0.0001	0.0633	< 0.0001
FETAL MG VS. ADULT MG	0.9987	0.9431	0.1407	0.2995	> 0.9999	0.9998
COMPARISONS	**PROS1**	**APOE**	**SLCO2B1**	**SLC7A8**	**PPARD**	**CRYBB1**
CD14+ M VS. CD16+ M	0.8814	> 0.9999	0.9999	> 0.9999	0.4125	0.0011
CD14+ M VS. BLOOD DC	0.4077	0.9103	0.9994	0.9965	0.9185	0.6963
CD14+ M VS. IMGL	< 0.0001	< 0.0001	< 0.0001	< 0.0001	< 0.0001	< 0.0001
CD14+ M VS. FETAL MG	< 0.0001	< 0.0001	< 0.0001	< 0.0001	< 0.0001	< 0.0001
CD14+ M VS. ADULT MG	< 0.0001	< 0.0001	< 0.0001	< 0.0001	< 0.0001	< 0.0001
CD16+ M VS. BLOOD DC	0.9391	0.9455	0.9941	0.9987	0.138	0.0002
CD16+ M VS. IMGL	< 0.0001	< 0.0001	< 0.0001	< 0.0001	< 0.0001	< 0.0001
CD16+ M VS. FETAL MG	< 0.0001	< 0.0001	< 0.0001	< 0.0001	< 0.0001	< 0.0001
CD16+ M VS. ADULT MG	< 0.0001	< 0.0001	< 0.0001	< 0.0001	< 0.0001	< 0.0001
BLOOD DC VS. IMGL	< 0.0001	< 0.0001	< 0.0001	< 0.0001	< 0.0001	< 0.0001
BLOOD DC VS. FETAL MG	< 0.0001	< 0.0001	< 0.0001	< 0.0001	0.0004	< 0.0001
BLOOD DC VS. ADULT MG	< 0.0001	< 0.0001	< 0.0001	< 0.0001	< 0.0001	< 0.0001
IMGL VS. FETAL MG	0.0008	< 0.0001	0.2803	0.0127	0.091	> 0.9999
IMGL VS. ADULT MG	0.2533	< 0.0001	0.9909	0.4987	0.403	< 0.0001
FETAL MG VS. ADULT MG	0.1787	> 0.9999	0.7213	0.4966	0.9658	< 0.0001

Table S2

	Treatments[1]							
	Vehicle		IFNγ		IL-1β		LPS	
CYTOKINES	**mean ± SE**	**p-value**	**mean ± SE**	**p-value**	**mean ± SE**	**p-value**	**mean ± SE**	**p-value**
TNFA	2.56 ± 0.16	NA	58.82 ± 8.80	0.0008	29.74 ± 0.65	0.0471	116.49 ± 9.77	< 0.0001
IL6	0.00 ± 0.00	NA	12.22 ± 1.44	0.5649	13.92 ± 0.41	0.4736	274.39 ± 15.25	< 0.0001
IL8	339.21 ± 11.29	NA	3549.05 ± 181.22	< 0.0001	3,004.54 ± 47.58	< 0.0001	4,347.96 ± 75.61	< 0.0001
IL10	0.00 ± 0.00	NA	4.59 ± 2.35	0.1599	4.42 ± 1.33	0.1779	31.31 ± 1.52	< 0.0001
IL1A	1.59 ± 0.07	NA	1.48 ± 0.25	0.9999	4.89 ± 1.45	0.2535	30.55 ± 2.19	< 0.0001
CCL2	96.59 ± 6.27	NA	993.26 ± 55.76	0.0052	275.98 ± 19.54	0.7069	5,695.46 ± 275.72	< 0.0001
CCL3	104.91 ± 7.70	NA	295.39 ± 19.72	0.0043	556.24 ± 54.01	< 0.0001	0.00 ± 0.00	0.0807
CCL4	3,140.81 ± 165.84	NA	4,514.72 ± 10.01	< 0.0001	4,492.26 ± 51.35	< 0.0001	4,594.57 ± 33.96	< 0.0001
CXCL10	9.62 ± 1.48	NA	0.00 ± 0.00	0.1762	69.49 ± 4.73	< 0.0001	73.72 ± 4.53	< 0.0001
CCL17	4.70 ± 0.83	NA	25.82 ± 1.98	0.0168	21.75 ± 1.94	0.0464	92.96 ± 7.70	< 0.0001

Table S3

TREATMENTS[1]						
FAB		**BDTO**		**fAβ vs. BDTO**		
GENES	**Fold Change (over vehicle)**	**Genes**	**Fold Change (over vehicle)**	**Genes**	**Fold difference**	**p-value**
	mean ± SE		**mean ± SE**		**mean**	
MS4A6A	6.32 ± 0.32	**CD2AP**	4.62 ± 0.45	**MS4A6A**	4.731	< 0.0001
CD33	6.02 ± 0.41	**CLU**	3.84 ± 0.67	**CD33**	5.178	< 0.0001
ABCA7	5.79 ± 0.44	**BIN1**	2.56 ± 0.66	**ABCA7**	3.333	0.0014
TYROBP	4.99 ± 0.31	**ABCA7**	2.46 ± 0.70	**TYROBP**	3.756	0.0002
TREM2	4.86 ± 0.50			**TREM2**	3.426	0.0009
ZCWPW1	3.41 ± 0.42			**ZCWPW1**	2.610	0.0323
PTK2B	2.97 ± 0.16			**PTK2B**	2.483	0.0525
APOE	2.52 ± 0.19					
BIN1	2.34 ± 0.69			**CD2AP**	-4.144	< 0.0001
CLU	2.24 ± 0. 78					

[1]TREATMENTS: FAB (5 MG/ML) OR BDTO (5 MG/ML) 24 H.

Tables

Table 4: Top GO pathways enriched in Adult MG compared to Fetal MG and iMGLs.

Adult MG vs Fetal MG				Adult MG vs iMGL			
Description	**GO ID**	**LogP (-)**	**Log (q-value)**	**Description**	**GO ID**	**Log P (-)**	**Log(q-value)**
Extracellular matrix organization	0030198	38.10	-34.18	Regulation of cell migration	0030334	13.23	-9.58
Circulatory system development	0072359	36.87	-33.23	Regulation of cell adhesion	0030155	11.46	-8.12
Single organism cell adhesion	0098602	32.24	-29.04	Actin filament-based process	0030029	11.03	-7.78
Regulation of nervous system development	0051960	28.56	-25.55	Regulation of anatomical structure morphogenesis	0022603	10.95	-7.74
Regulation of cellular component movement	0051270	26.49	-23.54	Cell junction organization	0034330	10.29	-7.12
Adaptive immune response	0002250	25.87	-22.96	Enzyme linked receptor protein signaling pathway	0007167	9.73	-6.76
Response to cytokine	0034097	20.02	-17.49	Circulatory system development	0072359	8.59	-5.79
Epithelial cell proliferation	0050673	19.25	-16.74	Single-organism catabolic process	0044712	8.13	-5.42
Central nervous system development	0007417	19.12	-16.63	Oxidation-reduction process	0055114	7.78	-5.11
Negative regulation of cell proliferation	0008285	18.82	-16.34	Plasma membrane organization	0007009	7.35	-4.76
Tissue morphogenesis	0048729	18.50	-16.06	Cellular response to oxygen-containing compound	1901701	7.31	-4.73
Muscle structure development	0061061	17.98	-15.56	Negative regulation of cell proliferation	0008285	7.28	-4.72
Single organism cell adhesion	0050808	17.86	-15.48	Positive regulation of phosphorylation	0042327	7.14	-4.63
Regulation of nervous system development	0042063	17.26	-14.91	Renal system development	0072001	6.77	4.30
Regulation of Growth	0040008	16.62	-14.32				

Table 5: Top GO pathways enriched in Fetal MG compared to Adult MG and iMGL.

Fetal vs Adult MG				Fetal MG vs iMGL			
Description	**GO ID**	**LogP (-)**	**Log (q-value)**	**Description**	**GO ID**	**Log P (-)**	**Log(q-value)**
Leukocyte chemotaxis	0030595	6.92	-3.07	Single-organism catabolic process	0044712	10.41	-6.64
Response to acidic pH	0010447	4.07	-1.33	Regulation of cell migration	0030334	9.90	-6.26
Inorganic ion homeostasis	0098771	4.04	-1.31	Iron ion transport	0006826	8.68	-5.52
Regulation of cell migration	0030334	3.80	-1.18	Divalent metal ion transport	0070838	8.44	-5.34
Circulatory system process	0003013	3.72	-1.13	Carbohydrate metabolic process	0005975	7.39	-4.59
Melanosome organization	0032438	3.70	-1.13	Small GTPase mediated signal transduction	0007264	6.69	-3.99
Anion transport	0006820	3.54	-1.01	Angiogenesis	0001525	6.64	-3.97
Macrophage migration	1905517	3.47	-0.95	Positive regulation of transport	0051050	6.15	-3.59
Transmembrane receptor protein tyrosine kinase signaling pathway	0007169	3.23	-0.81	Positive regulation of intracellular signal transduction	1902533	6.12	-3.57
Negative regulation of receptor activity	2000272	3.14	-0.76	Aminoglycan metabolic process	0006022	6.03	-3.50
Positive regulation of phagocytosis, engulfment	0060100	3.13	-0.76	Cell projection assembly	0030031	5.81	-3.31
Sterol import	0035376	3.13	-0.76	Cell-substrate adhesion	0031589	5.68	-3.21
Behavior	0007610	3.11	-0.75				
Positive regulation of transport	0051050	3.02	-0.70				
Vesicle organization	0016050	2.96	-0.65				

Table 6: Top GO pathways enriched in iMGL compared to Fetal MG and Adult MG.

iMGL vs Fetal MG				iMGL vs Adult MG			
Description	**GO ID**	**LogP (-)**	**Log (q-value)**	**Description**	**GO ID**	**LogP (-)**	**Log(q-value)**
Single organism cell adhesion	0098602	30.48	-26.23	Mitotic cell cycle process	1903047	28.46	-24.22
Mitotic cell cycle process	1903047	21.34	-17.87	Regulation of cell cycle	0051726	19.26	-15.94
Immune system development	0002520	18.56	-15.55	DNA replication	0006260	17.22	-14.09
Regulation of cellular component movement	0051270	16.11	-13.32	Chromatin organization	0006325	11.44	-8.64
Mitotic cell cycle phase transition	0044772	15.94	-13.18	Regulation of nuclear division	0051783	11.25	-8.47
Leukocyte migration	0050900	15.19	-12.49	Immune system development	0002520	10.90	-8.15
Taxis	0042330	14.76	-12.12	DNA-dependent DNA replication	0006261	10.22	-7.51
Positive regulation of cell differentiation	0045597	14.76	-12.12	Negative regulation of transcription from RNA polymerase II promoter	0000122	10.20	-7.50
Inflammatory response	0006954	14.64	-12.03	Microtubule cytoskeleton organization	0000226	9.96	-7.27
Anatomical structure formation involved in morphogenesis	0048646	13.83	-11.27	Leukocyte activation	0045321	9.57	-6.94
Positive regulation of cell proliferation	0008284	13.82	-11.26	Regulation of small GTPase mediated signal transduction	0051056	9.16	-6.56
Positive regulation of intracellular signal transduction	1902533	12.20	-9.73	Cell cycle G2/M phase transition	0044839	9.01	-6.44
Positive regulation of hydrolase activity	0051345	11.80	-9.35	Signal transduction by p53 class mediator	0072331	8.47	-5.99
Negative regulation of multicellular organismal process	0051241	11.67	-9.23	Regulation of transcription involved in G1/S transition of mitotic cell cycle	0000083	8.34	-5.88
Negative regulation of cell proliferation	0008285	11.62	-9.18	Cellular response to oxygen-containing compound	1901701	8.15	-5.73

Experimental Procedures

Reagents

All cell culture flasks, reagents, supplements, cytokines, and general reagents were purchased from ThermoFisher (Carlsbad, CA) unless otherwise noted.

Maintenance and Culture of Human Pluripotent Stem Cells (hPSCs)

All stem cell work was performed with approval from UC Irvine Human Stem Cell Research Oversight (hSCRO) and IBC committees. Use of human tissue was performed in accordance and approval of Institutional Review Board (IRB). Human iPSC cell lines ADRC 5,F5, F14,22, and 76 (control subjects) were generated by the UCI ADRC Induced Pluripotent Stem Cell Core using non-integrating Sendai virus (Cytotune). iPSCs were confirmed to be sterile, karyotype normal by G-banding, and pluripotent via Pluritest (UCLA) Analysis. iPSCs were maintained feeder-free on matrigel (MTG) in complete TeSR-E8 medium (Stemcell Technologies) in a humidified incubator (5% CO_2, 37^{o}C).

Differentiation of iPSCs to Hematopoietic Progenitor Cells (iHPCs)

Human iPSC derived hematopoietic progenitors were generated using defined conditions with several modifications to previously published protocols (Kennedy et al., 2007, Sturgeon et al., 2014). Briefly, iPSCs were triturated to generate a single-cell suspension and seeded in tissue-culture treated 6-well plates at 5 x 10^5 cells/cm^2 in E8 medium + Y-27632 ROCK Inhibitor (10 μM; R&D Systems). Cells were cultured for 24 hours under normoxic (20% O_2) conditions after which the E8 media was changed to differentiation media composed of a base media: IMDM (50%), F12 (50%), insulin (0.02 mg/ml), holo-transferrin (0.011 mg/ml), sodium selenite (13.4 μg/ml), ethanolamine (4 μg/ml), L-ascorbic acid 2-Phosphate magnesium (64 μg/ml; Sigma), monothioglycerol (400 μM), PVA (10 μg/ml; Sigma), Glutamax1XGlutamax (1X), chemically-defined lipid concentrate (1X), non-essential amino acids (NEAA; 1X), Penicillin/Streptomycin (P/S;1%), and completed with factors: FGF2 (50 ng/ml), BMP4 (50 ng/ml), Activin-A (12.5 ng/ml), and LiCl (2mM) in hypoxia (5%O_2). After two days, media was changed to

base media supplemented with FGF2 (50 ng/ml) and VEGF (50 ng/ml). On day 4, media was changed to media containing FGF2 (50 ng/ml), VEGF (50 ng/ml), TPO (50 ng/ml), SCF (10 ng/ml), IL-6 (50 ng/ml), and IL-3 (10 ng/ml). On Day 6, media was supplemented with medium. Cells were cultured for an additional 4 days (10 days total), after which, $CD43^+$ cells were isolated by FACS for iMGL differentiation. Additionally, iPSC-derived HPCs (Cellular Dynamics) were identified as a commercial source of $CD43^+$ progenitors.

Generation of Microglia-like Cells from iHPCs

$CD43^+$ iHPCs were plated in Matrigel-coated 6-well plates (BD Biosciences) with serum-free complete differentiation media at a density of 1-2 $x10^5$ cells per well. Differentiation media consists a base media: phenol-free DMEM/F12 (1:1), insulin (0.2 mg/ml), holo-transferrin (0.011 mg/ml), sodium selenite (13.4 µg/ml), B27 (2% v/v), N2 (0.5%, v/v), monothioglycerol (200 µM), Glutamax (1% v/v), Non-Essential Amino Acids (1% ,NEEA) and additional insulin (4 µg/ml; Sigma). Complete differentiation media includes M-CSF (25 ng/ml), IL-34 (100 ng/ml; Peprotech), and TGF□-1 (50 ng/ml; Militenyi) added just before feeding cells. Cells were supplemented with complete differentiation media every two days. At day 12, early iMGLs were collected (300x *g* for 5 mins at 25ºC) and a 50% media change was performed. After 25 days of microglial differentiation (35 days from iPSC), iMGLs were cultured in complete differentiation media supplemented with CD200 (100 ng/ml, Novoprotein) and CX3CL1 (100 ng/ml; Peprotech) for an additional three days before use in studies.

Human Adult and Fetal Microglia Isolation

Human microglia were isolated from adult brain tissue using previously described protocols(Durafourt et al., 2013). Briefly, normal appearing cortical tissue was resected from pharmacologically intractable non-malignant cases of temporal lobe epilepsy. Tissue was cleaned extensively and mechanically dissociated. A single cell suspension was generated following gentle enzymatic digestion using trypsin and DNAse prior to passing through a nylon mesh filter. Single cell suspension underwent a fickle ultracentrifugation step to remove myelin. Dissociated cells were centrifuged, counted,

and plated at $2x10^6$ cells/mL in MEM supplemented with heat-inactivated FBS (5%), P/S (0.1% v/v) and glutamine (0.1% v/v.). Microglia were grown for 3 days, collected and plated at $1x10^5$ cells/mL and maintained in culture for 6 days during which time cells received two treatments of TGFβ (20 ng/mL) on days 3 and 5. Human fetal brain tissue was obtained from the Fetal Tissue Repository (Albert Einstein College of Medicine, Bronx, NY). Total RNA was isolated using standard Trizol (Invitrogen) protocols and stored at−80 °C.

3D Brain-Organoid Cell Culture

Human 3D brain organoids were generated as previously described with some modifications (Lancaster et al., 2013) with modifications. iPSCs were cultured and maintained on Vitronectin XF (Stem Cell Technologies) in 6-well tissue culture treated plates (BD Falcon) and maintained with TeSR-E8 media (Stem Cell Technologies) daily, at 37°C with 5% CO_2. At approximately 80% confluency, iPSCs were detached from the Vitronectin XF substrate using the standard ReLeSR protocol (Stem Cell Technologies) and centrifuged, pelleted, and suspended in embryoid body (EB) media, which consists of KO DMEM/F12 (Invitrogen), KOSR (20% v/v), Glutamax (1% v/v), NEAA (1X), 2-Mercaptoethanol (0.1mM), bFGF (4 µg/ml), and HSA (0.1% v/v) and ROCK inhibitor (50 µM), to form EBs. Approximately $1x10^4$ cells were plated per well of a standard V-bottom 96-well plate coated with Lipidure (1% v/v; AMSBio) to avoid having the EBs attach to the 96-well plate. After 4 days in EB media with bFGF (4 ng/ml) and ROCK inhibitor (50 µM), both the bFGF and ROCK inhibitor were discontinued leaving the brain organoids in basic EB media for an additional 3 days (7 days total). After the EB media phase, the EB media is replaced with neural epithelium (NE) media which consists of DMEM/F12, N2 supplement (0.1% v/v), Glutamax (1% v/v), MEM-NEAA (0.1% v/v), Heparin solution (0.2mg/ml; Sigma), and filtered using 0.22 □m PES filter (EMD Milipore). The brain organoids were transferred to an ultra-low attachment 24-well plate (Corning) using cut P200 pipette tips, with 1-2 EBs per well in 1 ml NE media. The EBs were neuralized in the NE media for five days, after which they were transferred into Matrigel (Corning) using a mold created from siloconized parafilm and a sterile empty P200 box. The brain organoids were kept in a 6 cm suspension petri dish with differentiation media

consisting of KO DMEM/F12 (50%), Neurobasal medium (50%), N2 supplement (0.1% v/v), B27 without vitamin A supplement (0.1% v/v), Insulin solution (0.1% v/v; Sigma), 2-Mercaptoethanol (0.1mM), Glutamax (1% v/v), MEM-NEAA (1% v/v), and Penicillin/Streptomycin (0.1% v/v). After five days of being exposed to differentiation media containing B27 without vitamin A, the differentiation media was replaced by a formulation that is identical except for the replacement of B27 without vitamin A to B27 with vitamin A; at this time point, the brain organoids are also transferred to a 125 ml spinning flask bioreactor (Corning) siliconized with Sigmacote (Sigma), where they were fed differentiation media with vitamin A weekly for 8 weeks. After 12 weeks, Borgs were utilized for iMGL co-culture studies.

RNA-seq library construction

Cells were harvested and washed three times with DPBS and stored in RNAlater, RNA preservation solution. RNA was extracted from all cell types using RNeasy Mini Kit (Qiagen) following manufacturer's guidelines. RNA integrity (RIN) was measured for all samples using the Bioanalzyer Agilent 2100 series. All sequencing libraries analyzed were generated from RNA samples measuring a RIN score ≥ 9. The Illumina TruSeq mRNA stranded protocol was used to obtain poly-A mRNA from all samples. 200 ng of isolated mRNA was used to construct RNA-seq libraries. Libraries were quantified and normalized using the Library Quantification Kit from Kapa Biosystems and sequenced as paired-end 100 bp reads on the Illumina HiSeq 2500 platform.

RNA-seq analysis

RNA-seq reads were mapped to the hg38 reference genome using STAR(Dobin et al., 2013) aligner and mapped to Gencode version 24 gene annotations using RSEM(Li and Dewey, 2011). Genes with expression (< 1 FPKM) across all samples were filtered from all subsequent analysis. Differential gene expression analysis was performed on TMM normalized counts with EdgeR (Robinson et al., 2010). Multiple biological replicates were used for all comparative analysis. A p-value ≤ 0.001 and a 2-fold change in expression were used in determining significant differentially expressed genes for respective comparisons. PCA analysis was performed using the R package rgl and

plotted using plot3d. Clustering was performed using R hclust2 and visualized using Java Tree View 3.0 (http://bonsai.hgc.jp/~mdehoon/software/cluster/software.htm).

Confocal Microscopy and Bright field Imaging

Immunofluorescent sections were visualized and images captured using an Olympus FX1200 confocal microscope. To avoid non-specific bleed-through each laser line was excited and detected independently. All images shown represent either a single confocal *z*-slice or *z*-stack. Bright field images of cell cultures were captured on an Evos XL Cell Imaging microscope.

Flow Cytometer Analysis

Cells were suspended in FACs buffer (1X DPBS, 2% BSA, and 0.05mM EDTA) and incubated with human Fc block (BD Bioscience) for 15 min at 4°C. For detection of microglial surface markers, cells were stained with anti CD11b-FITC clone ICRF44, anti CD45-APC/Cy7 clone HI30, anti CX3CR1-APC clone 2A9-1, anti CD115-PE clone 9-4D, and anti CD117-PerCP-Cy5.5 clone 104D2, ZombieViolet™ live/dead stain , all from Biolegend (San Diego, CA). Cells were run on FACs Aria II, FACs Aria Fusion (BD Biosciences) and data analyzed with FlowJo software (FlowJo).

Cytospin and May-Grunwald Giemsa Stain

$1x10^5$ cells were suspended in 100 µl of FACs buffer and added to Shandon glass slides (Biomedical Polymers) and assembled in a cytology funnel apparatus. Assembled slides containing cells were loaded in a cytospin instrument and centrifuged (500 rpm, 5 min). Slides were allowed to air-dry for two minutes and immediately stained in May-Grunwald stain (100%; Sigma) for 5 min. Next, slides were washed in PBS for 1.5 min and immediately placed in Giemsa stain (4%; Sigma) for 20 min at room temperature. Slides were washed in double-distilled water 6 times and allowed to air-dry for 10 min. Slides were preserved using glass coverslips and permount (Sigma).

RNA Isolation and qPCR Analysis

Cells were stored in RNAlater stabilizing reagent and RNA was isolated using Qiagen RNeasy Mini Kit (Valencia, CA) following manufacturer's guidelines. qPCR analysis was performed using a ViiA™ 7 Real-Time PCR System and using Taqman qPCR primers.

Rat Cortical and Hippocampal Neuron Isolation

All procedures were performed under an IUCAC approved protocol. Primary cortical and hippocampal neuron cultures were derived from embryonic rat (E18) as previously described (Loo et al., 1993). Briefly, dissected tissue was dissociated with trypsin, triturated, and plated on 6-well plates coated with poly-L-lysine coated in NB medium (serum-free Neurobasal supplemented with1% B27. Cells were plated at a density of 5 × 10^6 cells/ml and maintained in culture until used.

iMGL Co-culture with Rat Neurons

Rat hippocampal or cortical neurons were cultured for 21 days with 50% media change every 3-4 days. iMGLs were cultured with neurons at a 1:5 ratio (1 x10^6 iMGL to 5 x 10^6 neurons) in 50% iMGL and 50% NB medium. After 3 days, iMGLs were collected for RNA isolation.

iMGL Transplantation in MITRG Mouse Brain.

All animal procedures were performed in accordance with NIH and University of California guidelines approved IAUC protocols (IAUC #2011-3004). MITRG mice were purchased from Jax (The Jackson Laboratory, #017711) and have been previously characterized (Rongvaux et al., 2014). MITRG mice allow for xenotransplantation and is designed to support human myeloid engraftment. iMGLs were harvested at day 38 and suspended in injection buffer: 1X HBSS with M-CSF (10 ng/ml), IL-34 (50 ng/ml), and TGFβ-1 (25 ng/ml). iMGLs were delivered using stereotactic surgery as previously described (Blurton-Jones, et al, 2009) using the following coordinates; AP: -0.6, ML: ± 2.0, DV: -1.65. Brains were collected from mice at day 60 post-transplantation per established protocols (Blurton-Jones, et al, 2009). Briefly, mice were anesthetized using sodium-barbiturate and perfused through the left-ventricle with cold 1X HBSS for 4 min.

Perfused mice were decapitated and brain extracted and dropped-fixed in PFA (4% w/v) for 48 hours at 4°C. Brains were then washed 3 times with PBS and sunk in sucrose (30% w/v) solution for 48 hours before coronal sectioning (40 µm) was performed using a microtome (Leica). Free-floating sections were stored in PBS sodium azide (0.05%) solution at 4°C until IHC was performed.

Immunocytochemistry and Immunohistochemistry

For ICC, cells were washed three times with DPBS (1X) and fixed with cold PFA (4% w/v) for 20 min at room temperature followed by three washes with PBS (1X). Cells were blocked with blocking solution (1X PBS, 5% goat or donkey serum, 0.2% Triton X-100) for 1 h at room temperature. ICC primary antibodies were added at respective dilutions (see below) in blocking solution and placed at 4°C overnight. The next day, cells were washed 3 times with PBS for 5 min and stained with Alexa Fluor® conjugated secondary antibodies at 1:400 for 1 h at room temperature in the dark. After secondary staining, cells were washed 3 times with PBS and coverslipped with DAPI-counterstain mounting media (Fluoromount, southern Biotech). For BORG IHC, tissue were collected and dropped-fixed in PFA (4% w/v) for 30 min at room temperature and then washed three times with PBS. BORGs were then placed in sucrose solution (30% w/v) overnight before being embedded in O.C.T (Tissue-Tek). Embedded tissue was sectioned at 20 µm using a cryostat and mounted slides were stored at -20°C until staining. For BORG staining, mounted tissue was removed from storage and warmed by placing at room temperature for 30 min. Tissue were rehydrated and washed with room temperature PBS (1X) 3 times for 5 min. Heat-mediated antigen retrieval was performed by using Citrate Buffer (10mM Citrate, 0.05% Tween 20, pH=6.0) at 97°C for 20 min and then allowed to cool to room temperature. After antigen retrieval, slides were washed three times with PBS. Slides were then washed once in PBS-A solution (1X PBS with 0.1% Triton X-100) for 15 min. Tissue was blocked using PBS-B solution (PBS-A, 0.2% BSA, and 1.5% goat or donkey serum) for 1 h at room temperature. After block, primary antibodies were added to PBS-B solution (250-350 µl/ slide) at appropriate dilutions (see below) and incubated overnight at room temperature. The next day, slides were washed with PBS-A solution 3 times for 5 min each. Tissue were

blocked for 1 h using PBS-B solution at room temperature. After block, slides were incubated with Alexa Fluor® conjugated secondary antibodies (all at 1:500) and Hoechst stain (1X) in PBS-B (for 250-300 µl/slide) for 2 h at room temperature in the dark. After secondary staining, slides were washed 5 times with PBS for 5 min. Slides were cover slipped using fluoromount (Southern Biotech). For mouse brain IHC, brains were collected, fixed, and processed as mentioned above. Free-floating sections were blocked in blocking solution (1X PBS, 0.2% Triton X-100, and 10% goat serum) for 1 h at room temperature with gentle shaking. For human TMEM119 staining, heat mediated antigen retrieval was performed prior to blocking, as performed previously (Bennett et al., 2016). Free-floating tissue antigen retrieval was performed by placing floating sections in a 1.5 ml micro centrifuge tube containing 1 ml of Citrate Buffer solution and placing in a pre-heated temperature block set at 100^{o}C. Tissue was heated for 10 min at 100^{o}C then removed and allowed to come to room temperature for 20 min before washing with PBS 3 times for 5 min and then proceeding with blocking step. For AD mouse brain staining of amyloid plaques, floating sections were placed in 1X Amylo-Glo ® RTD^{TM} (Biosensis) staining solution for 10 min at room temperature without shaking. After staining, sections were washed in PBS 3 times for 5 minutes each and briefly rinsed in MiliQ DI water before being placed back in to PBS followed by blocking. Primary antibodies were added to staining solution (1X PBS, 0.2% Triton X-100, and 1% goat serum) at appropriate dilutions (see below) and incubated overnight at 4^{o}C with slight shaking. The next day, sections were washed 3 times with PBS and stained with Alexa Fluor® conjugated secondary antibodies at 1:400 for 1 h at room temperature with slight shaking in the dark. After secondary staining, sections were washed in PBS 3 times for 5 min and mounted on glass slides. After mounting, slides were cover slipped with DAPI-counterstain mounting media (Fluoromount, southern Biotech). Primary antibodies:

mouse anti-β3Tubulin (1:500; Biolegend, 801201)

mouse anti-human Cytoplasm (SC121,1:100; Takara Bio Inc., Y40410),

chicken anti-GFAP (1:500; Abcam, ab4674)

rabbit anti-Iba1 (1:500; Wako; 019-19741)

goat anti-Iba1(Abcam; 1:100, ab5076) * use only Alexa Fluor 488 or 555 secondary antibody.

mouse anti ITGB5 (1:500;Abcam, ab177004)

mouse anti MMP-9 (1:500; EMD Millipore, AB19016)

mouse anti-human MerTK (1:500; Biolegend, #367602)

rabbit anti-P2RY12 (1:125; Sigma; #HPA014518)

rabbit anti-PROS1 (1:500; Abcam, # ab97387)

rabbit anti-PU.1 (1:500; Cell Signaling Technology, 2266S)

rabbit anti-human TMEM119 (1:100; Abcam, ab185333)

goat anti-human TREM2 (1:100; R&D Systems, AF1828)

TGFβR1 (1:500,Abcam, ab31013).

ADP migration and calcium imaging assays

Trans-well migration assays to ADP was performed as previously described(De Simone et al., 2010, Moore et al., 2015). iMGLs ($5.5x10^4$ cells/well) were cultured in serum-free basal media without cytokines for 1hour. Next, iMGLS were pre-exposed to DMSO or PSB0739 (50 μM, Tocris) for 1hr at 37ºC in 5% CO_2 cell culture incubator. Cells were then washed three times with basal medium and plated in trans-well migration chambers (5 μm polycarbonate inserts in 24 wells; Corning) containing Adenosine 5'-phosphate (ADP, 100 μM; Sigma) in the bottom chamber in 37ºC in 5% CO_2. After 4 hours, cells were washed three times and fixed in PFA (4%) for 15 minutes at room temperature. Cells were stained with Hoechst stain for 10 mins to visualize nuclei of cells. A blinded observer counted total cells per slide and then scrubbed cells off top surface, washed with PBS, and recounted to record migrated cells. Migration was reported as migrated over total cells per well. Fluorescent images of cells were captured using Olympus IX71 inverted microscope.

For calcium imaging, iMGLs were plated on poly-L-lysine-coated coverslips and 1 hour later were incubated with Fura-2-AM (Molecular Probes) calcium dye diluted in Ringer solution containing (in mM): NaCl 140, KCl 4.5, $CaCl_2$ 2, $MgCl_2$ 1, HEPES 10, glucose

10, sucrose 5, pH=7.4. After 1-hour incubation the dye was washed out 3 times using Ringer solution and treated for 1 hour with either P2ry12 inhibitor PSB0739 (50 µM, Tocris) or Vehicle (DMSO) and used for experiments. Baseline Ca^{2+} signal (I_{340}/I_{380}) were measured for more than 100 s and then ADP (10 µM) was introduced under stead flow after baseline measurement. Ca^{2+} recordings were performed on Zeiss (Axiovert 35)-based imaging setup and data acquisition was conducted with Metafluor software (Molecular Devices). Data analysis was performed using Metafluor, Origin Pro, and Prism 6.0.

Phagocytosis Assays

iMGLs and MD-M□, were incubated with mouse anti CD16/32 Fc-receptor block (2 mg/ml; BD Biosciences) for 15 minutes at 4°C. Cells were then stained with anti CD45-APC clone (mouse cells; Tonbo Biosciences; San Diego, CA) at 1:200 in flow cytometer buffer. Samples were then analyzed using Amnis Imagestreamer^{x} Mark II Imaging Flow Cytometer (Millipore). *E.coli*, human synaptosome, fAβ, and BDTO phagocytosis was analyzed using the IDEAS software onboard Internalization Wizard algorithm. Additive free Anti-CD11b antibody (Biolegend, #301312) was used for CD11b blockade.

Fibrillar A□ Preparation.

Fibrillar fluorescent amyloid-beta ($fA\beta_{1-42}$) was generated as described previously (Koenigsknecht-Talboo and Landreth, 2005). Fluorescently labeled Aβ peptide (Anaspec; Fremont, CA) was first dissolved in NH_4OH (0.1%) to 1 mg/ml, then further diluted to 100 µg/ml using sterile endotoxin-free water, vortexed thoroughly, and incubated at 37°C for 7 days. fAβ was thoroughly mixed prior to cell exposure.

BDTO Preparation

Brain-derived tau oligomers were purified by immunoprecipitation as described previously (Lasagna-Reeves et al., 2012). Tau oligomers were isolated by immunoprecipitation with the T22 antibody using PBS-soluble fractions of homogenates prepared from AD brain. These were then purified by fast protein liquid chromatography (FPLC) using PBS (pH 7.4). Additional analyses include Western blots to detect

contamination with monomeric tau or large tau aggregates (tau-5, normally appear on top of the stacking gel) and using a mouse anti-IgG to identify non-specific bands. BDTOs were subsequently conjugated to pHrodo-Red per manufacturer's protocol.

Human synaptosomes

The synaptosome preparation protocol was adapted from (Gylys et al., 2000). Human tissue samples were obtained at autopsy and minced, slowly frozen in 0.32 M sucrose with 10% DMSO and stored at −80 °C. To obtain a crude synaptosome fraction, tissue was thawed in a 37 °C water bath and homogenized in 10 mm Tris buffer (pH 7.4) with proteinase inhibitors (Roche) and phosphatase inhibitors (Sigma-Aldrich) using a glass/Teflon homogenizer (clearance 0.1–0.15 mm). The homogenate was centrifuged at 1000 *g* at 4 °C for 10 min, the supernatant was removed and centrifuged again at 10 000 *g* at 4 °C for 20 min. Resulting pellets were suspended in sucrose/Tris solution and stored at −80 °C. Synaptosomes were conjugated to pHrodo-Red per the manufacturer's protocol.

Mesoscale Multiplex Cytokine and Chemokine Assay

iMGLs culture media was replaced with basal media for 2 hours prior to stimulation with IFNγ (20 ng/ml), IL1β (20 ng/ml), and LPS (100 ng/ml) for 24 hours, after which cells were collected for RNA and conditioned media assessed for cytokine secretion. To simultaneously assess multiple cytokine and chemokine analytes from iMGL conditioned media, conditioned media from each treatment group was processed and analyzed using the V-PLEX human cytokine 30-plex kit (Mesoscale) per the manufacturer's protocol.

Isolation of PBMCs and Monocytes from Human Blood

Human blood samples were collected from healthy donors through the UCI ICTS Blood Donor Program with approved IRB. Human peripheral blood mononuclear cells (PBMCs) were isolated from healthy donors using Ficoll-paque (GE Healthcare) gradient separation. In brief, blood was layered on top of Ficoll-Paque and centrifuged in swinging bucket rotator without brake (400x *g*, 40 minutes, 18°C). After

centrifugation, plasma and upper layers were removed and PBMCs isolated from the interphase. Cells were then washed once with ice-cold PBS and used immediately. CD14 and CD16 monocytes were isolated via negative selection from PBMCs using the EasySep™ Monocyte Enrichment Kit (Stemcell Technologies) per manufacturer's instructions. Isolated cells were washed three times with PBS and sorted by FACs for either RNA-sequence analysis or used for further macrophage differentiation.

Monocyte-derived Macrophages

Isolated monocytes were plated onto tissue culture treated 6-wells at 2 x10^6 cells/ml in RPMI-1640 media at 37°C 5%CO_2 incubator. After two hours, media was aspirated to waste and adherent monocytes washed three times with DPBS and replaced with complete media composed of RPMI-1640, FBS (10% v/v), Penicillin/streptomycin (1% v/v), L-alanyl-L-glutamine (2mM). To generate MD-M, M-CSF (25 ng/ml) was added to wells and cells differentiated for 5 days.

AD-GWAS qPCR Primers

The following validated and available Taqman primers were used: APOE Hs00171168_m1, CR1 Hs00559342_m1, CD33 Hs01076281_m1, ABCA7 Hs01105117_m1, TREM2 Hs00219132_m1, TREML2 Hs01077557_m1, TYROBP (DAP12) Hs00182426_m1, PICALM Hs00200318_m1, CLU Hs00156548_m1, MS4A6A Hs01556747_m1, BIN1 Hs00184913_m1, CD2AP Hs00961451_m1, CASS4 Hs00220503_m1, MEF2C Hs00231149_m1, DSG2 Hs00170071_m1, MS4A4A Hs01106863_m1, ZCWPW1 Hs00215881_m1, INPP5D Hs00183290_m1, and PTK2B Hs00169444_m1.

Statistical Analysis

Statistical analysis was performed using Graphpad Prism 6 software. Comparisons involving more than two groups utilized one-way ANOVA followed by Tukey's *post hoc* test and corrected p-values for multiple comparisons were reported. Comparison's with

more than two groups and comparing to a control or vehicle group utilized one-way ANOVA followed by Dunnett's *post hoc* test with corrected p-values for multiple comparisons reported. Two-Way ANOVA were followed by Sidak's multiple-comparison *post-hoc* test Comparisons of two groups utilized two-tailed Students t-test. All differences were considered significantly different when $p<0.05$. Statistical analysis for RNA-sequencing is detailed above and all other statistical analysis are reported in the figure legends.